CHALMERS
UNIVERSITY OF TECHNOLOGY

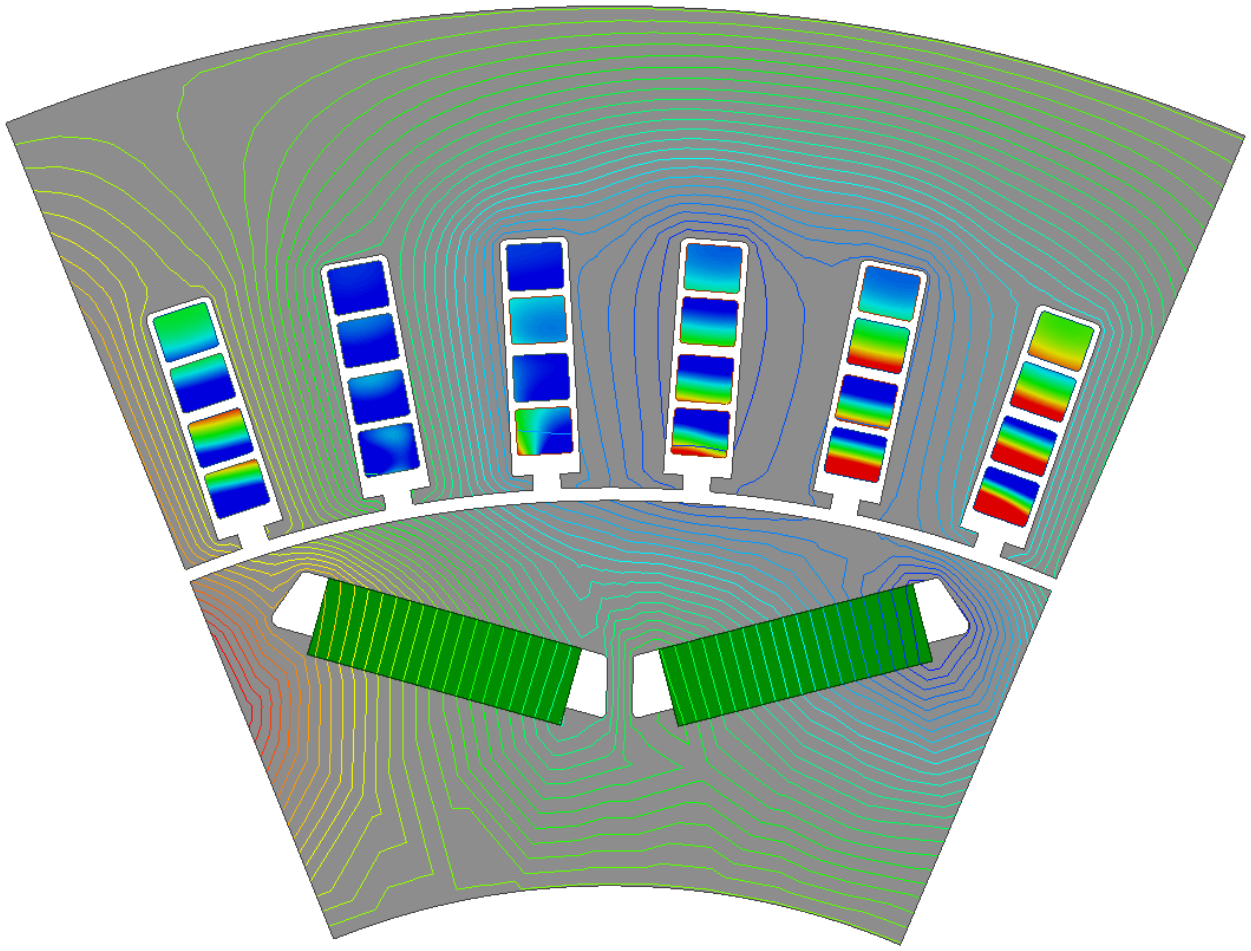

FEA study of proximity effect in hairpin windings of a PMSM for automotive applications

Master's thesis in Electrical power engineering

DAVID DEURELL
VIKTOR JOSEFSSON

Department of Electrical Power Engineering
CHALMERS UNIVERSITY OF TECHNOLOGY
Gothenburg, Sweden 2019

Master's thesis

FEA study of proximity effect in hairpin windings of a PMSM for automotive applications

David Deurell
Viktor Josefsson

CHALMERS
UNIVERSITY OF TECHNOLOGY

Department of Electrical Power Engineering
Chalmers University of Technology
Gothenburg, Sweden 2019

FEA study of proximity effect in hairpin windings of a PMSM for automotive applications
David Deurell
Viktor Josefsson

Supervisor: Selam Chernet, Volvo Car Corporation
Supervisor: Torbjörn Larsson, Volvo Car Corporation
Supervisor: Sonja Lundmark, Department of Electric Power Engineering
Supervisor: Jian Zhao, Department of Electric Power Engineering

Examiner: Yujing Liu, Department of Electric Power Engineering

Master's Thesis
Department of Electric Power Engineering
Chalmers University of Technology
SE-412 96 Gothenburg
Telephone +46 31 772 1000

Typeset in LaTeX
Gothenburg, Sweden 2019

FEA study of proximity effect in hairpin windings of a PMSM for automotive applications

David Deurell
Viktor Josefsson
Department of Electrical Power Engineering
Chalmers University of Technology

Abstract

The electrification of the vehicle fleet is increasing the demand for highly efficient and cheap electric traction motors. One way of meeting this demand could be to use hairpin windings in the motors. This technique has recently gained interest in literature and is also used by some manufacturers.

The hairpin winding uses rectangular copper bars in order to achieve a high fill factor. This has beneficial effects for thermal properties and also gives an increased power density. However, the larger cross sectional area increases the frequency dependant eddy current loss. The conventional machine winding using round random winding consists of many small circular conductors, therefore the frequency dependent loss is reduced. However, the non frequency dependent loss is higher since it has a lower fill factor.

The primary aim of this thesis is to investigate the frequency dependant copper loss in a hairpin interior permanent magnet synchronous machine. The study is based on a machine that was recently bought by the division of Electric Power Engineering at Chalmers University of Technology. The study of copper losses also looks at the impact of changing some design parameters, namely, stator slot opening and the number of conductors.

The study is performed by finite element method simulations in Ansys Maxwell. The thesis separates different phenomena contributing to the total copper loss by isolating different effects by simulating several modified motor models. The results are then compared to a simplified analytical calculation. The study shows that the major part of the losses are caused by the proximity effect between the conductors in one slot.

A comparison is made by simulating the same machine design with the two different types of winding. This shows that the hairpin winding is to prefer at lower frequencies while the random winding is better at higher frequencies. To be more general a frequency sweep of 1-2000Hz is performed. The losses at the maximum speed, from the data sheet of this machine, show an increase in loss of 93.2% for the hairpin and 3.7% for the round random winding. At base speed the increase of loss is 16.8% for hairpin and 0.9% for round random winding. Since the fill factor decides the non frequency dependent loss the round random winding starts at a higher loss.

The loss distribution between conductors in one slot containing conductors from one phase shows that the distribution of loss becomes more uneven the more the

speed increase. At the maximum design speed the conductor closest to the yoke has around 13% of the total loss of the slot and the conductor closest to the air gap holds 42%.

Keywords: Hairpin winding, Bar winding, IPMSM, Eddy current loss, Proximity effect, Skin effect, Copper loss, FEA.

Acknowledgements

First of all we would like to thank Volvo Cars Corporation together with Chalmers University of Technology for giving us the opportunity to perform the study leading up to this thesis report.

We would like to thank Selam Chernet and Torbjörn Larsson at Volvo Car Corporation for interesting discussions and support during this thesis.

We would also like to thank Sonja Lundmark, Jian Zhao and Yujing Liu at Chalmers for our weekly meetings where we have had the opportunity to discuss technical questions and the progress of the thesis.

Viktor Josefsson, Gothenburg, June 2019
David Deurell, Gothenburg, June 2019

Glossary

AC Alternating Current.

DC Direct Current.

EESM Electrically Excited Synchonous Machine.

FEA Finite Element Analysis.

IPM Interior mounted Permanent Magnet.
IPMSM Interior mounted Permanent Magnet Synchronous Machine.

KCL Kirchoff's Current Law.

MMF Magnetomotive Force.
MTPA Maximum Torque Per Ampere.
MTPV Maximum Torque Per Volt.

PM Permanent Magnets.
PMSM Permanent Magnet Synchronous Machine.
PWM Pulse Width Modulation.

SPM Surface mounted Permanent Magnet.
SyRM Synchronous Reluctance Machine.

UCD Uniform Current Distribution.

Contents

1
Introduction

1.1 Background

The increasing number of electric vehicles is forecast to reach a 30% market share in 2030 according to [1]. This will increase the demand for highly efficient electric traction motors. Increased efficiency for electric machines can be achieved in different ways, in this thesis report the focus will be on the copper losses in the stator winding of a hairpin Permanent Magnet Synchronous Machine (PMSM).

The main machine of interest in this project is a hairpin PMSM with hairpin winding technology. Hairpin windings consist of pre-shaped copper bars that are bent into a so called "hairpin shape" as shown in Figure 1.1. The hairpin winding may provide manufacturing advantage when the mounting technology is matured and the cost is decreased. Since the technology is rather new, as stated in [2], the mounting time is uncertain but may show signs of fast improvement.

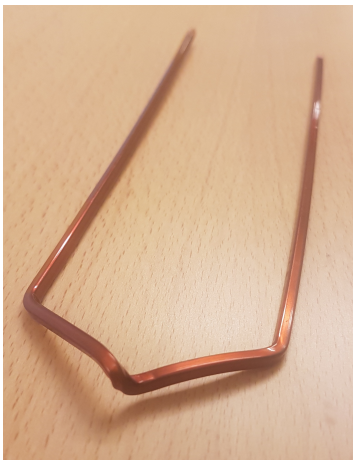

Figure 1.1: Typical pre-shaped hairpin copper bar from Chalmers' hairpin machine.

These copper bars, or hairpins, are then inserted into the stator slots, the legs of the copper bar is then bent again and welded together with another hairpin to form a coil. The coils are then connected in a particular pattern to form a winding, a fully assembled and welded three phase hairpin stator is shown in Figure 1.2

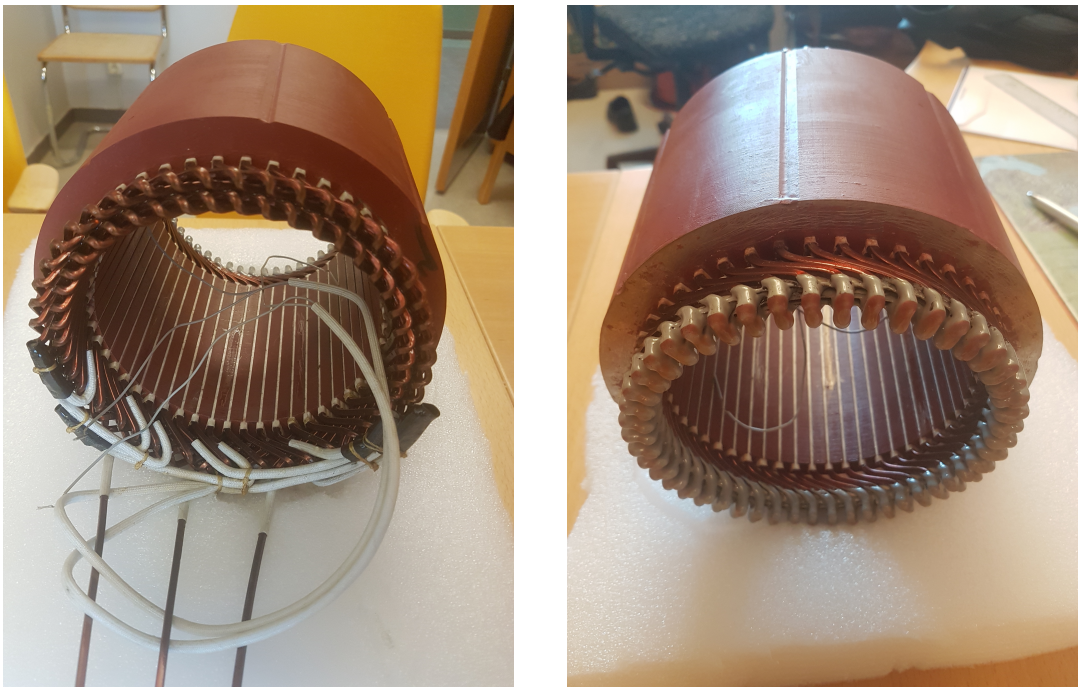

Figure 1.2: Fully assembled hairpin stator from Chalmers' hairpin machine, the topside is shown on the left together with external connections and bottom welded side on right.

Due to the assembling process being one sided, it may offer some additional design properties for the stator, such as the possibility to fully close the stator slots. This since the copper bar is placed in the stator slot by pushing it through, along the stator height, and not inserted through the slot opening into the slot. This could be compared with various insert winding techniques, where the copper wires has to enter the slot through the slot opening. One example of this is the conventional "random round winding" which will be used as a comparison in the report.

Since the winding does not have to go through the slot opening it can easily be made as a single, or a few, copper strands with larger area, compared to the round random winding. This results in more copper area per slot, i.e. larger fill factor, since packing several small strands with individual insulation results in less copper area than for one larger strand. This since there will be some unusable space between conductors and also since there will be more insulation compared with the amount of copper.

Due to the larger amount of copper area the hairpin winding offers some advantages. It gives lower copper losses which means that more current can be drawn from the motor, which results in a higher power density, at low speed (frequency). At high speed the large area is not beneficial, since it leads to larger induced currents resulting in proximity effect and eddy current loss [3]. In [4] it has been shown that in order to mitigate the losses at high speed the conductors can be segmented. However, continued segmentation would mean that the fill factor of the hairpin machine would approach the fill factor of the round winding machine and thus

losing the low speed advantages. The study made in [4] also showed that the copper losses are the largest loss contributor at load. Therefore the designer of the traction motor needs to design the machine knowing where the highest efficiency is needed and for this operating point reduce the copper losses, which [2] showed in a design approach.

Since copper is a good heat conductor the higher fill factor has preferable thermal properties, so it can conduct heat through the conductors to the stator body, which can be cooled [5]. At lower frequencies, if the size of the stator slots is kept unchanged and if the fill factor is higher, the current density in the wires will decrease for the same amount of current passing per phase in the stator, which leads to lower heat production, which is also beneficial for the thermal properties.

Since the hairpin machine has high power density [6], the stator tooth-tips can be made wider, but still keeping the same power as for a round winding machine. This can decrease the spatial harmonics since the variations in air gap flux is smaller. The decreased flux variation leads to lower torque ripple. The decrease in harmonics also leads to lower iron losses and less vibration and noise [6].

As mentioned previously in the background there are several design options with different characteristics, each with its own benefits. This thesis will focus on the electrical characteristics of copper losses in the hairpin winding and the impact of some of the design options.

The machine that will be the center of this study is a hairpin PMSM ordered by Chalmers. The intended use of the machine is to be placed in a test vehicle that is being built at the division of electrical power engineering. It is designed for 400V, peak power (30s) is 60kW and average power is 30kW.

1.2 Aim

The aim of this thesis is to study the frequency dependant losses, and the underlying phenomena, in the hairpin machine. To put this into perspective these losses are compared with the characteristics of the losses of a random round winding machine. This comparison will be performed by Finite Element Analysis (FEA) in Ansys Maxwell. Since the hairpin design offers the possibility to vary the slot opening, the impact of different slot openings on the resistance is studied. To further improve the understanding of the frequency dependent losses in the hairpin machine an investigation of the impact of number of layers is also performed.

Therefore the aim is defined as:

- Make a FEA model of the machine to estimate induced copper losses for different frequencies and loads. Find the current distribution and estimate the ratio between loss for Alternating Current divided by Direct Current (AC/DC) losses.

  - Research and investigate underlying phenomena behind loss increase and its distribution between wires due to eddy effects.

- Perform a comparison of frequency dependant copper losses between hairpin winding and random round winding.
  - Rebuild hairpin model into round winding FEA model.

- Investigate how the slot opening and number of conductors per slot affect the resistance.

1.3 Limitations

- To simplify analysis only sinusoidal current excitation is used. This provides for a current without harmonics but it decreases simulation time. The absence of harmonics decreases losses but it simplifies the analysis of physical phenomena.
- The impact of end winding elements such as resistance and inductance is neglected since a 2D model is used and the end windings is not simulated. Several other studies show both simulated results and analytical approaches on how to estimate the resistance and inductance of the end windings. The impact on the results will be that the total loss is smaller and that the quotient of AC/DC resistance is higher if the increase of resistance is lower in the end windings than in the active part. In [7] it is said that the increase of resistance in the end winding part is low compared to in the active part.
- The random round winding machine which is used as a comparison for AC losses is not optimised. From the authors point of view this is not something that is particularly important, since the focus is on the increase of losses and not magnitude of losses for the round winding machine. The main impacts are noted in the text when comparing the results with the hairpin machine.
- No measurements are performed in order to verify the simulations. The measurements are not performed due to that the delivery of the machine and the power electronic inverter were delayed.
- Field weakening is neglected. To simplify simulations field weakening and thus voltage limits is not considered. Instead the influence of angle and magnitude of the current is studied separately.

1.4 Sustainable development and ethics

To be able to lower CO2 emissions more vehicles will need to be electrified. This puts pressure on higher efficiency batteries and electric motors. The benefit with a study like this is that it may offer the possibility to manufacture motors with higher efficiency.

PMSM often use rare earth magnets like neodymium for their magnetic performance. The biggest producer of neodymium magnets today is China [8]. To be dependent

on one producer is not optimal, when this producer also has a questionable approach to human rights an ethics problem arise.

During the mining of neodymium heavy metals are emitted in to the ground water which is a environmental and safety issue for people in the area around the production site[8]. Neodymium is present in reserve around the world but regulation and safety constraints are increasing the price which is allowing China to maintain the position as the largest exporter of the magnets. [8].

Other solutions with motors that are not using permanent magnets are a possible way around, however these are having a lower efficiency making them less suitable for vehicle applications.

2

PMSM Theory

This chapter will introduce the theory of PMSMs. It will start by explaining fundamental electromagnetic theory and definitions, these will then be used to explain the working principle of a PMSM. First a simple model will be used, after that more complex theory will be added about the motor and later on the losses related to PMSM are explained. In the end of this chapter FEA is explained since it will be used in the simulations.

2.1 Fundamental electromagnetic relations

In this section fundamental electromagnetic relations will be introduced in order to understand the phenomena happening in an electric machine and to support the discussion in the results chapter.

Magnetic fields are needed in order to enable the conversion from electric power to mechanical power. The magnetic field may be created by different sources such as permanent magnets (PMs) or by a current as can be described here by Ampere's law as

$$\oint_l \boldsymbol{H} \cdot dl = I_{encl} = NI \tag{2.1}$$

where I_{encl} is the free enclosed current of the line integral, N is the number of turns of a coil and I is the current. The final product of NI may be referred to as magnetomotive force (MMF). If I_{encl} is an alternating current then the resulting magnetic field is alternating. The magnetic field direction is decided by the right hand rule, which means that if the current is in the direction of the thumb then the magnetic field is in direction of the fingers of a closed hand. The magnetic field always creates closed paths.

Inside a material where bound current is present magnetic flux density $\boldsymbol{B}$ is calculated by the constitutive relation of magnetic fields as

$$\boldsymbol{B} = \mu_0 \mu_r \boldsymbol{H} = \mu \boldsymbol{H} \tag{2.2}$$

where μ_0 is the magnetic permeability in vacuum and μ_r is the relative magnetic permeability of the material, the permeability is usually written as $\mu = \mu_0 \mu_r$. The relation of permeability is usually strongly non linear for magnetic material.

Another term used is the magnetic flux Φ that is created by the magnetic field and describes how much magnetic flux that is flowing in a particular cross section by

$$\Phi = \int_A \boldsymbol{B} \cdot dA \tag{2.3}$$

where the integral is taken over the area of interest. The amount of magnetic flux is decided by the strength of the source of the magnetic field, by Ampere's law, also limited by the reluctance in the medium of which it flows.

So far only relations regarding magnetic phenomena has been discussed. In order to relate the magnetic and electric field in the machine Faraday's law and Lenz's law is used

$$\nabla \times \boldsymbol{E} = -\frac{d\boldsymbol{B}}{dt} \tag{2.4}$$

where $\boldsymbol{E}$ is the electric field. For calculations in the machine Faraday's law can be simplified into

$$\mathcal{E} = -N\frac{d\Phi}{dt} = -\frac{d\Psi}{dt} \tag{2.5}$$

where $\mathcal{E}$ is an induced voltage and Ψ is the flux linkage. The flux linkage represent the magnetic flux that flows through a coil of N turns if the magnetic flux passes all turns. Faraday's law is used to describe both back-EMF in the machine and induced eddy currents, which will be discussed later in the chapter. In the case for eddy currents, N is not applicable and is therefore equal to one. For both these cases the induced voltage will resist change in current and therefore also change in magnetic flux due to the minus sign of Lenz's law.

Due to the non uniform current density $\boldsymbol{J}$ caused by the induced eddy currents Ohm's law for field quantities is given by

$$\boldsymbol{J} = \sigma \boldsymbol{E} \tag{2.6}$$

where σ is the conductivity of the material.

2.2 PMSM theory

Several different types of electrical machines exists, they are usually split in to two categories AC, alternating current, machines and DC, direct current, machines. The AC machines can then be divided in to synchronous and asynchronous machines, the synchronous machines can further be divided into PMSM, permanent magnet synchronous machines, and non PM machines, which contains Electrically Excited Synchronous Machines (EESM), Synchronous reluctance Machines (SyRM) etc. In this project the PMSM will be used, the PMSM has a three phase AC wound stator and a rotor that has permanent magnets.

A simplified model of the stator in a three phase electrical machine is shown in Figure 2.1, in the figure the windings for phase A, B and C are placed 120° apart from each other resulting in a pattern as A, C', B, A',.. where the prime represent the opposite direction. The current in A, B, C is sinusoidal with direction in to the paper and is also shifted 120° in time between phases.

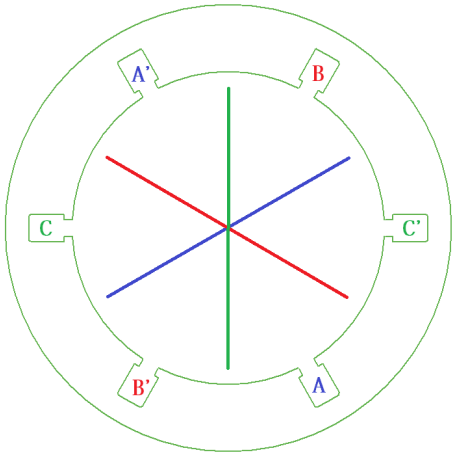

Figure 2.1: Simplified illustration of a 2 pole stator with a three phase winding and the resulting rotating magnetic field.

This sequence of placing the windings produces a rotating magnetic field according to the right hand rule of Ampere's law 2.1. The pole pair set up by A and A' will create a magnetic field vector principally in the direction of the blue line. The vector will oscillate back and forth along the the line, which is perpendicular to the line through A and A' with the same frequency as the current. The same will be true for the two other pole pairs B-B' and C-C' as in Figure 2.1 but in the red and green direction, respectively. The flux generated by the windings are as follows

$$\begin{aligned}\Phi_A &= \Phi\sin(\omega t)\cos(\alpha)\\ \Phi_B &= \Phi\sin(\omega t - \tfrac{2}{3}\pi)\cos(\alpha - \tfrac{2}{3}\pi)\\ \Phi_C &= \Phi\sin(\omega t + \tfrac{2}{3}\pi)\cos(\alpha + \tfrac{2}{3}\pi)\end{aligned}$$

where Φ represent the magnitude of the flux which is the same for all phases if everything is symmetrical. The sine expression represent the current time shift. The cosine represent the geometrical position of the coordinate system where α is the the angle between phase A and the defined coordinate system. If these three vectors are added, the time shift of phases and the positions of the windings will create a rotating magnetic field vector with constant amplitude as

$$\Phi_A + \Phi_B + \Phi_C = \frac{3}{2}\Phi\sin(\omega t - \alpha)$$

by the help of some mathematical rules. This simple model of a rotating magnetic field may be updated with more slots per phase, a higher number of poles.

The rotor in a permanent magnet machine may have different topology, it can use Surface mounted Permanent Magnets (SPM), and Interior mounted Permanent

Magnets (IPM), in this project the assigned motor is an IPM. The IPM has both reluctance torque and electromagnetic torque since the interior magnets has significantly different permeability then the surrounding iron [9]. Since the IPM has both reluctance and electromagnetic torque it is related with the SyRM. In Figure 2.2 different synchronous motors are shown with their torque characteristic depending on the amount of magnets and their placement. A PMSM with IPM may be designed with different amount of magnets, a machine that use only a small amount of magnets is usually called permanent magnet assisted synchronous reluctance motors.

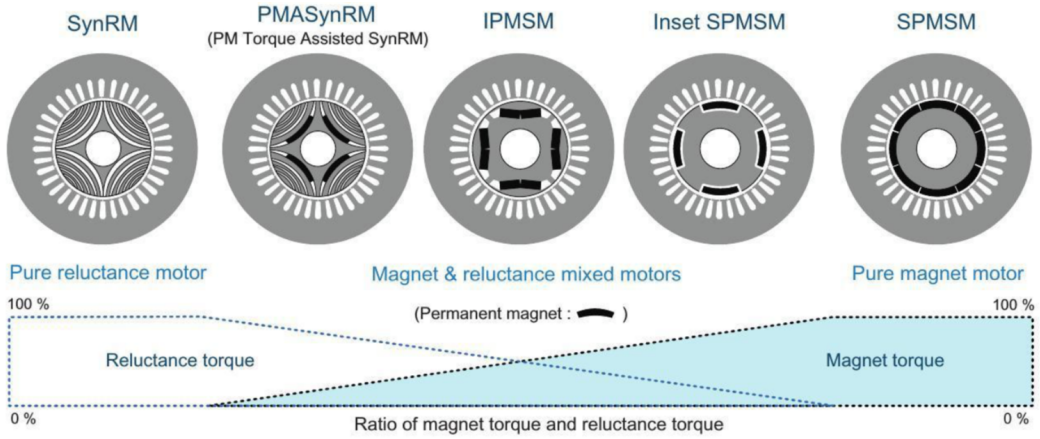

Figure 2.2: Different rotor topologies for PM motors and reluctance motors and the amount of torque from reluctance and permanent magnets. Figure from K. Sang-Hoon in [9].

The purpose of the magnets in the rotor is to latch on to the rotating magnetic field of the stator. Therefore it needs to have the same amount of poles as the stator. Since the rotor is supposed to latch on to the stator rotating magnetic field a variable frequency drive is needed. Otherwise, if the frequency would be to high, or if the load on the machine is to high, then the attracting force between stator magnetic field and PM field would be to weak and the rotor would not gain high enough speed before the two magnetic fields would start to repel each other, this would result in zero net torque.

For the simple illustration of the motor above with two poles, one electrical period will correspond to one full rotation of the magnetic field in the stator. For a motor with more than two poles, let's say four, one electrical period would not correspond to one full 360° turn of the magnetic field since two poles would be placed on one semicircle and the other two on the other half of the circle, this would decrease the mechanical speed to half of the frequency of the electrical input. The output speed of the synchronous motor would then follow the generic expression

$$\Omega = \frac{60f}{P} \tag{2.7}$$

where Ω is the mechanical output speed in Rotations Per Minute (rpm), f is the electrical frequency of the input and P is the number of pole pairs.

2.3 Mathematical model of the PMSM

When working with PMSMs it is common to use the dq-coordinate system, the dq system is a rotating reference system. In this system the time varying quantities will behave as DC components. It is also advantageous in order to explain the reluctance torque, since reluctance torque is based on the difference in reluctance in different directions, namely d and q axis. The d axis is in the direction of the main magnetisation axis. A typical circuit diagram in dq-coordinates used for analysing PMSMs is shown in Figure 2.3 [6].

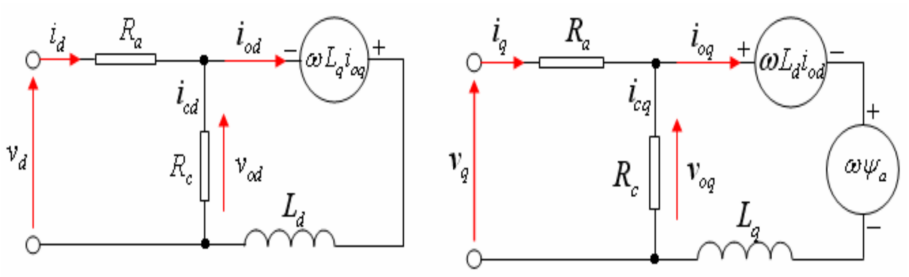

Figure 2.3: A common circuit model in dq-coordinate system. To the left is the circuit model for d axis and to the right is the circuit model for q-axis. Figure from D. Jung et al. in [6].

In the figure R_a represent all the resistive losses in the machine by

$$R_a = R_{dc} + R_{ac} + R_{end} \tag{2.8}$$

where R_{dc} is the resistive losses due to the current magnitude, R_{ac} is the resistive losses due to AC phenomena that will be discussed in Section 2.6.1 and *Rend* is the losses in the end windings. Another resistive element in the circuit is R_c, which represent the core loss in the iron rotor and stator.

Other circuit parameters are L_d and L_q, which are the inductance in d and q direction respectively. There is also one frequency dependent cross coupling term from L_q on the v_d voltage and vice versa. The last parameter Ψ_a represent the flux linkage from the permanent magnet and is also frequency dependant for the voltage.
According to [10] the torque is given by

$$T = \frac{3}{2}P(\Psi_a i_q + (L_d - L_q) i_d i_q) \tag{2.9}$$

where P is the number of pole pairs and the first 3/2 depends on which kind of dq-transformation that is used.

The total torque in the machine is generated by two parts, reluctance and PM torque as mentioned in Section 2.2. In (2.9) the first term represent the torque from the permanent magnets and the second term represent the torque from the reluctance. The resulting torque for a specific voltage and current is dependant on the angle between current and voltage and can be controlled by the frequency inverter. The

two parts contributing to the torque do not usually generate maximum torque at the same angle. A typical torque-angle characteristic for an IPMSM is shown in Figure 2.4. A result of the angle dependency on torque is that the initial rotor position needs to aligned with the poles created by the currents in the winding. Since the magnets is responsible for the induced back-EMF the initial angle has an impact here as well.

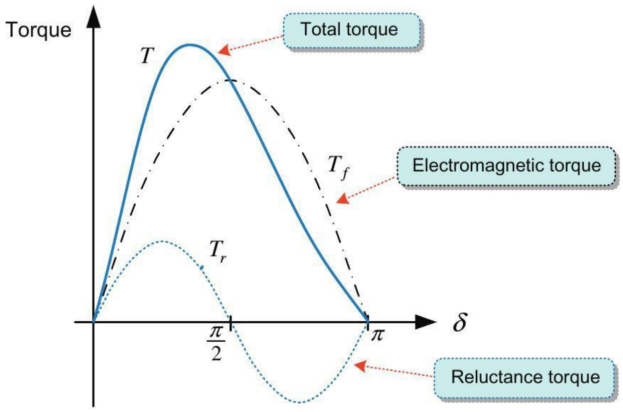

Figure 2.4: Shows a typical torque-angle characteristics for an IPMSM. Figure from K. Sang-Hoon in [9].

The machine's torque and power is further limited by a voltage maximum in order to protect the conductor insulation, it is also current limited due to thermal constraints. Another important aspect for the machine is to operate the machine at the best possible operating point, which is denoted by Maximum Torque Per Ampere (MTPA) shown in Figure 2.5. In the figure the MTPA curve is shown as the blue line which represent the current vector, when this line cross the $T_{e\max}$ the current limit is reached. Parallel curves may be drawn below to the $T_{e\max}$ curve and it is the crossing by this curve that defines the MTPA line. In this figure the speed is low and the voltage ellipse represented by the dotted line is outside of the limiting current circle.

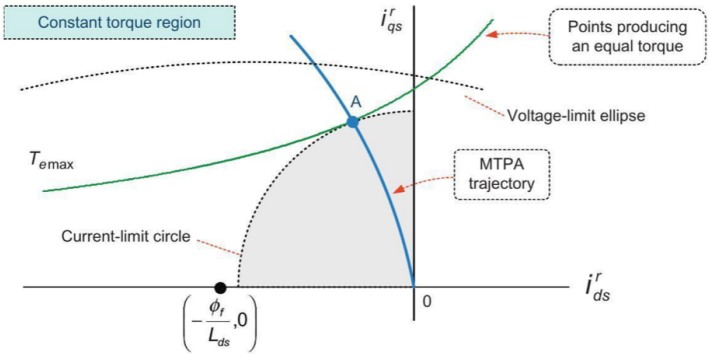

Figure 2.5: Shows the MTPA curve including the limiting current maximum and voltage ellipse. Figure from K. Sang-Hoon in [9].

When the voltage limit is hit at the MTPA curve due to large induced back-EMF

caused by high speed, the control is usually switched to Maximum Torque Per Volt (MTPV) denoted by the blue line in Figure 2.6. The figure shows a typical curve that can be used to have maximum torque at given operating point with limiting current circle and voltage ellipse.

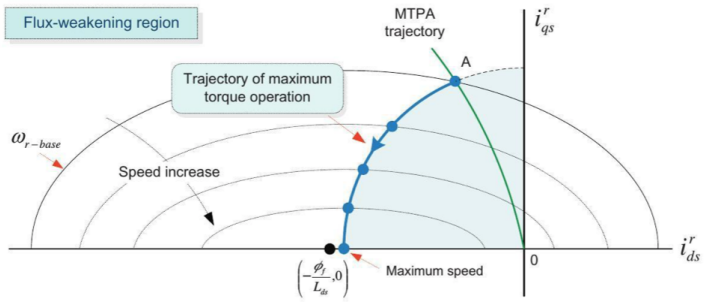

Figure 2.6: Shows the MTPA curve including the limiting current maximum and voltage ellipse. Figure from K. Sang-Hoon in [9].

Another useful curve for an IPMSM is the torque-speed curve shown in Figure 2.7. In the figure two zones are visible, the constant torque region and the constant power region, in both regions the current is constant and may have a magnitude of the current maximum. In the first region voltage continues to increase as the speed increase up until the second region starts and voltage limit is reached. In the second region where power is constant the voltage is not allowed to increase anymore. Then MTPV has to be applied leading to a decrease of torque due to a changed current angle. Usually also a third region is used, the high speed region, in this region the current magnitude is decreased and the torque starts to decrease faster than in constant power region.

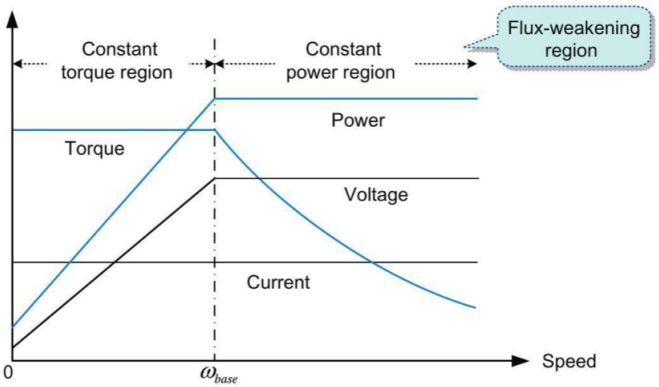

Figure 2.7: Shows torque-speed relation together with power characteristics. Figure from K. Sang-Hoon in [9].

One characteristic for permanent magnet motors is that they have *cogging torque*, also called no load torque. This phenomena means that if the motor, at no load, is turned, by hand for example, a torque will be noticed, cogging, as the motor shaft is rotated. The torque arise due to that the permanently excited rotor and its magnets

has a magnetic attraction to the stator teeth due to lower reluctance and therefore offer attraction and repelling force. The cogging torque over one period is shown in Figure 2.8 in which it can be observed that the torque vary around zero.

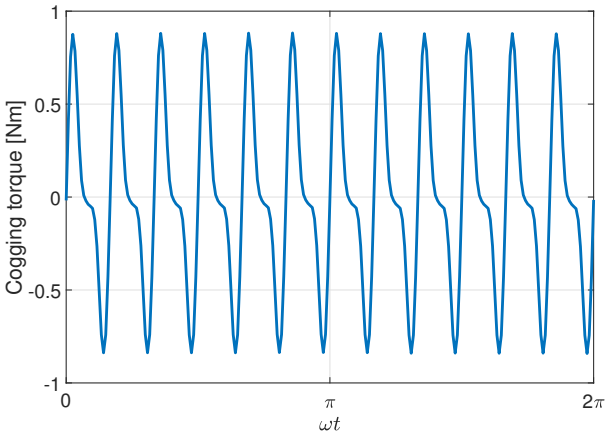

Figure 2.8: Shows cogging torque due the permanent magnets over one electrical period for the machine simulated in this thesis.

When the machine is operated at load condition this phenomena will add on top of the resulting torque as *torque ripple* and may be noticed in its application depending on motor control and inertia of the system.

In order to minimise the torque ripple *magnetic skewing* can be used in the rotor. This means that the magnets in the rotor are skewed sideways so that they does not align parallel to the teeth. This is implemented by segmentation of the magnets, which also makes them easier to handle when assembling the motor. The magnets are then positioned in a "staircase" shape and the skewing is performed in steps.

For a 2D model in FEM, the magnetic skewing can be implemented by offset angles of the initial rotor position. This method is implemented by setting an offset angle negative and do calculations, then the offset angle is set to positive and simulated and finally the result is averaged. In this method the average output torque would be similar to that of a real machine without doing a 3D model.

2.4 Different type of winding techniques

From Figure 2.1, which shows a simplified model of a stator, to an optimised motor many design decisions has to made. In this section a short discussion about design parameters for the distributed winding is performed. Only the distributed winding will be discussed since that is the one used for the studied machine. Besides geometrical parameters for the machine such as dimensions, slot shape etc. there are several design options for the winding.

To mention just a few important parameters there is number of slots, short pitching, number of slots per pole per phase, single or double layer winding etc. The choice

behind some of the design parameters may be that they are practical for manufacturing, other that they improve the behavior of the machine but sacrifice parts of the peak performance.

The number of slots in the machine depend on several factors, for example, the number of poles in the machine, single or double layer winding and how many slots per pole per phase that is needed. A large number of slots compared to the stator size may have a negative impact on iron saturation due to more narrow stator teeth.

Short pitch can be used to create a more sinusoidal terminal voltage by suppressing harmonics [11]. The short pitch would also have a reducing effect of the induced voltage.

The number of slots per pole per phase can be split up in different ways, for the machine in this project there are two slots per pole per phase. The conductors however are distributed with one half full slot, full slot and then a half full slot. Another way to distribute the phases would be to have two full slots next to each other. This could have an impact on copper loss due to the new field distribution and proximity effect. An increased number of slots per pole per phase would also have a reducing effect on the induced voltage magnitude. [11].

In a single layer winding, each coil would require two slots. Then if several number of slots per pole per phase is needed and also if the motor is supposed to have many poles, the total number of slots would be large. A large number of slots would result in more narrow teeth, which could lead to a large flux density in the teeth and saturation. Instead, for a two layer winding only half as many slots is needed compared to the single layer winding. When it comes to manufacturing a two layer winding are usually easier to build since it has a lower number of slots compared to the number of coils[11].

As mentioned in the background, two popular winding types for PMSMs, hairpin winding and random round winding will be simulated, where the random winding might be viewed as the more conventional one. The hairpin winding is explained in Section 1.1 but can shortly be summarised that it consists of a few large square copper bars per slot that is supposed to yield high fill factor in the slot.

The round random winding consists of many round conductor strands with individual area per strand that is significantly smaller than the area per hairpin bar. The machine is wound by putting a coil consisting of many turns into the slots of the machine. Each coil has two ends, one end is connected to another coil of the same phase and the other end connects to another coil in the other direction to form a winding. Except the first coil and the last coil of the winding, where one end will be used for incoming voltage and the other to connect to an Y or Δ-connection. The winding can may consist of a multiple series and parallel connection of coils to match current and voltage requirements. Partially finished random round winding is shown in Figure 2.9, the conductors leaving the motor are the ends that should be connected to other parts. In the figure also a coil is shown, it can be seen that it leaves one slot and entering another slot. Due to the cross section of the conductors

being smaller a benefit for this type of winding is that it is less affected by AC-loss at increasing frequency [2].

Figure 2.9: Partially finished winding of a stator. Figure from Todoservicios S.L. at [12]

2.5 Harmonics

Harmonics means that there are additional higher order frequencies which are multiples of the fundamental frequency of current and voltage in the system. The harmonics may be generated from several different sources such as electrical switching by transistors in converters, air gap spatial harmonics created from the machine itself due to slotting or iron saturation amongst other sources. Harmonics are usually unwanted and they usually increase copper loss since the current magnitude increase and therefore also thermal properties are affected, it also increase loss in iron and may have negative impact on torque.

In simulation the power supply to the machine can be chosen as current source or voltage source. If a sinusoidal current source is used the current will be pure sinusoidal and any generated harmonics will be forced to the voltage and opposite if voltage source is used.

2.6 Losses in a PMSM

In electrical machines there is several sources of loss, they are usually separated in to the following categories.

- Copper loss

- Iron loss and PM loss
- Mechanical loss
- Stray loss

As all loss lead to heat development, the loss is usually a critical design issue when it comes to design of electrical machines. Besides the thermal problems, power loss also cost money due to wasted energy and is also an environmental issue.

2.6.1 Copper losses

Copper losses is the term used for loss created from current that flows inside a conductor. It is dependant on the resistance and the current density. In the case of direct current (DC) the current distribution in the conductor is uniform and the loss is given by

$$P_{Cu} = I^2 R_{dc} \tag{2.10}$$

where I is the current and R_{dc} is the resistance. The DC resistance of a conductor is defined by

$$R_{dc} = \frac{l}{\sigma_c A} \tag{2.11}$$

where l is the length of the conductor, σ is the conductivity and A being the cross-sectional area of the conductor. The conductivity is a parameter of the material. For metals the conductivity decrease with increased temperature, this leads to a higher resistance for higher temperatures.

In case of alternating current (AC) in a conductor, the current distribution stops being uniform due to eddy effects and the loss is then given by

$$P_{Cu} = \frac{1}{\sigma} \int_{vol} \boldsymbol{J}^2 \cdot dV \tag{2.12}$$

where the integral represent the total medium of where the current is flowing, $\boldsymbol{J}$ is the current density and σ is the conductivity of the medium where the current is flowing.

For simplicity when calculating with AC, the non-uniform current distribution is avoided and instead replaced with the term R_{ac}. This new term is supposed to capture the behavior of the current distribution on average in the system and the current may be used for calculation. The AC resistance is defined by

$$R_{ac} = \frac{P_{ac}}{P_{dc}} R_{dc} = k \cdot R_{dc} \tag{2.13}$$

and is either used as R_{ac} or it can be used as a quotient that $R_{ac}/R_{dc} = k$, where k is equal to P_{ac}/P_{dc}.

2.6.1.1 Eddy currents

Eddy currents are induced current which are present in all parts of the machine, in the rotor and stator iron, the PMs and in the conductors. The eddy currents in conductors is as will be shown dependent on the cross sectional area of the conductors that is facing the magnetic flux, and the frequency of the machine, or speed since it is a synchronous machine [7]. Since the layout or cross sectional area is a contributing factor this is one of the things that separates the round winding and the hairpin winding from each other. The eddy currents is usually divided in two main categories when conductors is concerned, one is skin effect and concerns one single conductor, the other one is proximity effect which is when there are several conductors close to each other.

As stated in the beginning of the section eddy currents is an induced current, unlike useful induced current such as used in a transformer and in induction machines, the eddy currents is mainly related to losses or unwanted heating, although exceptions exist. As for all induced currents the eddy current is generated by an external or self-produced time varying magnetic field according to Faraday's law 2.5. The magnetic field could be generated by a moving magnet, or by a conductor according to Ampere's law 2.1. The difference in definition between useful induced currents and compared to eddy currents is that the sum of eddy currents is zero over one cross section and thus not forming a closed circuit. It only influences the current distribution in that particular cross section of the conductor and causes additional loss on top of the DC copper loss. Useful induced current utilised by the concept of a transformer is always forming a closed circuit and thus provide energy transfer. The eddy currents in iron creates a current and therefore loss in parts where no initial current is flowing.

2.6.1.2 Eddy currents in conductors

For eddy currents in conductors in the stator winding the eddy current loss, or AC-loss, is usually small in the end windings compared to the AC-loss in the active part of the machine due to the flux leakage through the slot [7]. In the active part eddy current will affect the current density and cause additional losses. This may create hot spots in parts of the windings which may age or damage the winding insulation and the motor may breakdown premature.

Eddy currents is usually divided in to two subcategories *skin effect* and *proximity effect* depending on the cause behind the new current distribution. The term skin effect is used to describe the phenomena when the applied current is forced to flow inside a thin layer of the conductor and it is also caused by its own magnetic field. It may be explained by current flowing in a round conductor placed in a straight line in space without interference from other sources. If current is applied to the conductor a magnetic field will be created around the conductor in circular paths and its magnitude and direction would be decided by Ampere's law in (2.1). Inside the conductor the magnetic field would increase up to the edge of the conductor, outside of the conductor the magnitude would decrease. If a AC current is applied the magnetic field would also be varying with the same frequency as the current,

then according to Faraday's law in (2.5) a voltage would be induced. If an arbitrary length of the radius inside the conductor is chosen, then since the magnetic field has a cylindrical shape, a current would be created rotating around this radius. Around the magnetic field at this radius a current would be created rotating around this imaginary circle in a direction so that the applied current is reduced in the middle of the conductor and increased in the skin of the conductor. Since the current distribution is changed the loss would increase by (2.12), a method used is to assign these losses to a new resistance R_{ac} as in (2.13). Since the current is confined into a smaller area, skin effect can be said to decrease the equivalent area of the conductor.

The skin depth for round conductors is given by

$$\delta = \sqrt{\frac{2}{\omega\mu\sigma}} \tag{2.14}$$

where ω is the frequency of the current in rad/s, μ i the permeability and σ is the conductivity. For square conductors the skin depth is proportional to δ [2]. In order to reduce skin effect, conductors with small cross sections compared to the skin depth should be used. For round conductors if the diameter d is $d < 2\delta$ skin effect will have low impact on the resistance according to [13].

When two or more current carrying conductors are in close proximity of each other, the magnetic field of one conductor will influence the other conductors, this is often referred to as proximity effect. In electrical machines this is of particular interest inside the slots in the stator. In the slots the conductors is placed closely together, sometimes with current of another phase, e.g another phase shift. This may cause a large redistribution of the current density depending on geometrical properties. In order to reduce the loss from proximity effect an optimal cross section towards the magnetic field should be chosen.

In [7] an analytical approximation for the effect of eddy currents is made, first for an u-shaped iron core with one solid conductor placed inside the core. Then it is elaborated to cover any number of conductors in width and height. Due to the shape of the iron core the magnetic field leakage would pass straight through the conductors and the current would have a distribution which would be in layers. The current distribution will increase in the top parts of the conductor and decrease in the bottom part. The reduced area, or increased loss, for this setup may be calculated by a reduced height factor according to [7]. Also in [7], the iron core is approximated by an infinite permeability, then by using (2.1), (2.5) and (2.6) and all the conductors are connected in series, then the equivalent reduced height of the conductor is derived to be

$$\xi = h_{cond}\sqrt{\frac{1}{2}\omega\sigma\mu\frac{b_{cond}}{b_{slot}}} \tag{2.15}$$

where h_{cond} is the height of the conductor, b_{cond} is the width of the conductor and b_{slot} is the width of the slot. Notice the resemblance in the equation compared with the equation for skin depth in (2.14).

In order to make use of (2.15), it needs to be adapted to fit a different number of conductors, not just a single conductor. In [7] it is stated that the solution is not dependant on how many conductors that is used in either direction of width and height. The equations used for calculating the resistance increase per conductor is

$$\varphi = \xi \frac{\sinh(2\xi) + \sin(2\xi)}{\cosh(2\xi) - \cos(2\xi)} \tag{2.16}$$

$$\psi = 2\xi \frac{\sinh(\xi) - \sin(\xi)}{\cosh(\xi) + \cos(\xi)} \tag{2.17}$$

where ξ from (2.15) uses the height and width of the individual conductors [7].

These equations is then used to calculate the height reduction factor for each layer by

$$k_{Rk} = \varphi(\xi) + k(k-1)\psi(\xi) \tag{2.18}$$

where k_{Rk} is the height reduction in the kth layer. The average height reduction is given by

$$k_R = \varphi(\xi) + \frac{z_t^2 - 1}{3}\psi(\xi) \tag{2.19}$$

where k_R represent the average height reduction or resistance increase and z_t is the number of layers in the height direction [7].

2.6.2 Iron and permanent magnet loss

Iron and PM loss consists of two types of losses, eddy current loss and hysteresis loss [13]. The eddy current loss is present in the permanent magnets, rotor and stator iron is due to the eddy effect as explained in Section 2.6.1.1.

Eddy currents that was introduced in 2.6.1.1 occurs in both the iron of the rotor and stator but also in the PMs as was mentioned. Again the loss arise due to Faraday's law 2.5 and the change of magnetic flux change. In order to reduce the eddy current loss the rotor and stator iron is laminated [13]. Lamination is done by stacking, thin disc sheets of iron electrically insulated from each other, together to the desired height of the stator or rotor. This reduce the loss by increasing resistance since the eddy currents would like to flow in paths parallel to the axial length.

The eddy current loss for permanent magnets are also reduced by making the magnet axial height shorter and thus increase resistance [7]. The permanent magnets are not made as short as for the sheets of iron since they have to be manufactured and mounted inside the machine.

Hysteresis loss can be explained by the B-H curve from an iron material shown in Figure 2.10. The relation between the magnetic field and magnetic flux density is non linear and their relation is called permeability as described in Section 2.1 by (2.2).

The hysteresis is a property of the material and may be explained by magnetised domains inside the magnetic material which originally are magnetised in random directions causing the material as a whole to lack any net magnetisation [14]. When a weak magnet field is applied, the volume of the domains whose magnetisation are in the same direction as the field grows, which increase the magnetic flux density, $\boldsymbol{B}$. A weak magnetic field is represented by $\boldsymbol{H}$ corresponding to point $P1$, at this low point of magnetisation, the magnetisation of the material is reversible and the volume of the domains may return to their initial volume. If the applied magnetic field is stronger than the one for point $P1$, then the change in domains is no longer reversible and the flux density will not return to the origin, this is known as hysteresis, a small hysteresis curve corresponding to points $P2$ and $P2'$ is shown within the large hysteresis loop containing $P3$ and $P3'$. At even higher applied field at point P3 the material becomes saturated which means that even with a higher applied field the increase of flux density is very limited with the increase of magnetic field. The line containing $O, P1, P2$ and $P3$ is called the *normal magnetisation curve*. On the B-H curve there are two more points which are of interest, namely, remanent flux density, $\boldsymbol{B_r}$, and $\boldsymbol{H_c}$, known as the coercive field intensity or coercive force. $\boldsymbol{B_r}$ represent how much the material has been magnetised when the external magnetic field is zero and is why permanent magnets exists, and $\boldsymbol{H_c}$ represent how much magnetic field that has to be applied to force the magnetic flux to zero.

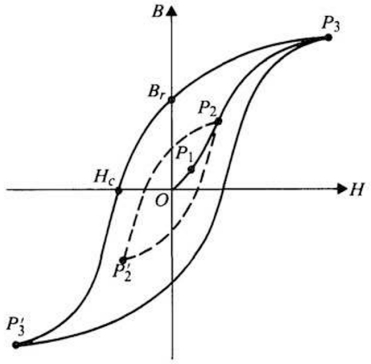

Figure 2.10: Typical B-H curve for an iron material. Figure from W. Chen et al. in [14].

The hysteresis loss can then be explained as friction between the changes in the domains inside the magnetic material [14]. The material has higher loss if the B-H curve has large $\boldsymbol{H_c}$, which increase the the frictional force which has to be overcome. For a current that is sinusoidal or changes direction, the magnetic field also varies between $\pm\boldsymbol{H}$, imply that the hysteresis loss is dependant of frequency. For an electrical machine the magnetic field changes direction along with the sinusoidal frequency, a magnetic material with small $\boldsymbol{H_c}$ and high flux density is desirable and is called *soft magnetic material* [14]. For a permanent magnet on the other hand a high $\boldsymbol{B_r}$ and large $\boldsymbol{H_c}$ is desirable to maintain a high magnetisation and to avoid demagnetisation, respectively. Also, due to losses in the magnets due to eddy currents or hysteresis loss in the magnets, or by other losses in a machine,

which create elevated temperatures, excessive temperatures needs to be avoided in the magnets to not cause demagnetisation.
According to [13] the hysteresis losses, in per unit, for iron can be calculated by

$$P_m = kf^a(B_{ac})^d \tag{2.20}$$

where k, a and d are material constants, f is the operating or switching frequency, $\boldsymbol{B_{ac}} = \hat{\boldsymbol{B}} - \boldsymbol{B_{avg}}$ where $\hat{\boldsymbol{B}}$ is the peak value and $\boldsymbol{B_{avg}}$ is the average value, for a PMSM $\boldsymbol{B_{avg}}$ is typically zero. In the simulations the loss in iron is calculated as the sum of (2.20) with different constants for eddy current, hysteresis and additional loss [15]. If the magnetic field has components of several frequencies due to harmonics, additional loss may occur due to the high frequency components.

2.6.3 Mechanical loss

In this section there will be a brief explanation of some of the most influential mechanical losses, such as windage loss and bearing friction.

Windage loss comprises of losses due to windage, for example machines which have a cooling fan and ventilation ducts. Another example is air turbulence which arise when the rotor rotates in the stator. The machine used in this project is water cooled around the stator and will therefore have low loss due to windage, since it does not have any ventilation ducts etc. According to [7] the windage loss depend on the drag force exerted on the rotor and the medium that surrounds the rotor. Also according to [7], equations to estimate the windage loss exists, this is done by approximating the rotor as a rotating cylinder with a surface roughness parameter and the losses on the ends of the rotor as two rotating disks in air if there are no fan wings on the edge of the rotor. The equations are strongly dependant on rotational speed, a power of three, and diameter, power of four for a cylinder and a power of five for the rotating disks.

Mechanical loss due to bearing friction depend on a number of parameters such as rotational speed, bearing type, size of the bearing, bearing load and which type of lubricant, the loss may be described by

$$P_{\text{mech, bearing}} = \frac{1}{2}\Omega\mu F D_{bearing} \tag{2.21}$$

where Ω represent the mechanical speed, μ is the friction in the bearing, F is the bearing load and $D_{bearing}$ is the bearing's inner diameter [7].

2.6.4 Stray loss

According to [7] iron loss is usually presented for no load iron loss and copper loss is presented as DC copper loss. Therefore losses due to harmonics and additional loss due to loading may be referred to as additional loss. In this report the loss in iron and copper is brought up in respective section. Other sources of additional loss for copper may be neglecting eddy effects in the end windings which also is a source of error. Also loss due to irregularities due to manufacturing of the motor may end up here.

3

Modelling and simulation setup of the PMSM

To be able to simulate the behaviour of the actual hairpin machine a model of the machine needs to be created. The simulations is done using finite element analysis which is performed in Ansys Maxwell. This chapter will present and motivate the simulation setup of the hairpin machine and the random round winding machine, which is used as a comparison. First the hairpin machine model will be presented and after that the random round winding machine. In all simulations the end winding impedance is neglected, this is due to that the impact of eddy effects in end windings is very small in comparison to active part [7]. The end winding impedance would have impact on several characteristics of the machine, like losses and induced voltage. Lastly, since the motor is symmetric, all simulations of both motors is done on one eighth of the full model to save simulation time.

3.1 Finite element analysis

Physical phenomena are often described by differential equations. Solving these differential equations over a geometry and over time is very time consuming. To handle these very big and advanced calculations the FEA is often used. This method discretizes the volume or area that is interesting in to specific calculation points. These points are spread out across the geometry building up a mesh of points where the differential equations are solved. How often the calculations at these mesh points are performed is decided by number of calculations per time period.

The two parameters, mesh points and calculations per time period, decides how accurate the results is. More calculations per time period and a higher number of mesh points is increasing the accuracy but also increases simulation time. Therefore a sensitivity analysis is performed to maintain a high accuracy while performing simulations as quick as possible.

3.2 FEA model of the hairpin machine

The following section introduces the model for the hairpin machine. It contains the geometrical dimension of the machine and also a motivation on the mesh set up and the number of steps used in simulations.

3.2.1 Motor parameters for the hairpin machine

In Table 3.1 the most important parameters of the machine can be seen. All values are collected from data sheet of the physical machine.

Table 3.1: Motor parameters

Parameter	Value	Unit
Number of slots	48	
Number of poles	8	
Number of phases	3	
Base speed	4100	rpm
Maximum speed	10000	rpm
Rated torque	70	Nm
Maximum torque	200	Nm
Maximum current	250	A_{rms}
Rated power	30	kW

In table 3.2 the physical dimensions of the machine is presented.

Table 3.2: Motor dimensions

Part	Dimension [mm]
Rotor diameter	121.6
Stator inner diameter	123
Stator outer diameter	175
PM width	14.17
PM height	4.27
Active length	120

To model the slots a standard type slot in Ansys Maxwell is used. The standard slot layout can be seen below in figure 3.1 with the corresponding dimensions in table 3.3.

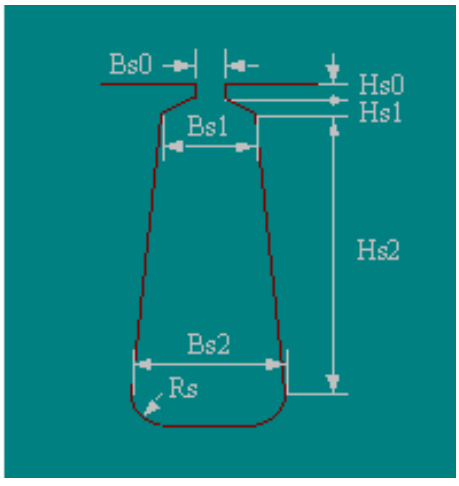

Figure 3.1: Standard slot in Maxwell [MAXWELL DOCUMENTATION]

Table 3.3: Slot dimensions

Part	Dimension [mm]
Hs0	0.8
Hs1	0
Hs2	12.4
Bs0	1.5
Bs1	3.7
Bs2	3.7
Rs	0.4

These configurations give the layout of the machine, without windings, that can be seen in figure 3.2. The model does not contain the inner part of rotor and shaft since it has negligible influence in the stator copper losses, this is again to shorten the simulation time.

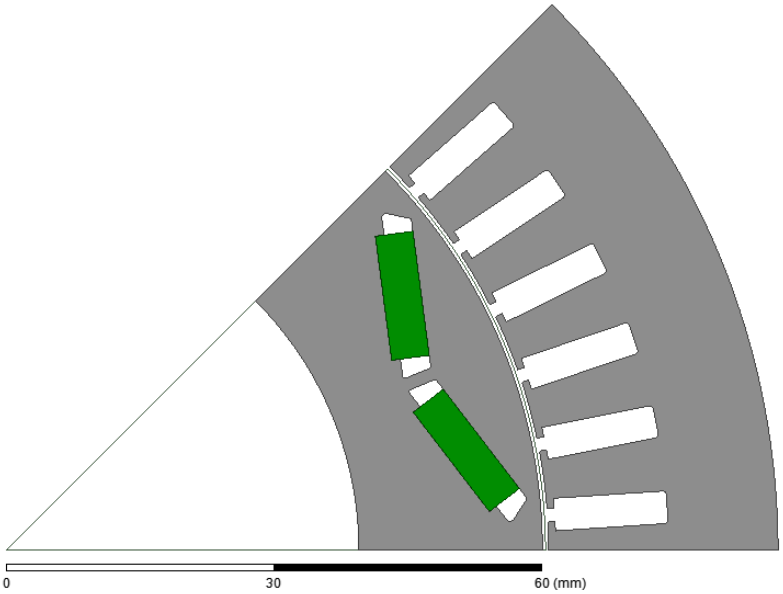

Figure 3.2: One eighth of the motor model. Permanent magnets in green, rotor and stator in grey.

Since this machine is supposed to model an actual machine the material used are specific materials from the manufacturer, they can be seen in Table 3.4. The permanent magnet material is a material based on NdFeB magnets. The rotor and stator core material is a sort of silicon steel.

Table 3.4: Motor materials

Part	Material
Conductors	Copper
Permanent Magnets	n35uh_2DSF1.000_X
Rotor and stator core	B35AV1900

3.2.2 Hairpin winding

The hairpin windings is implemented using the dimensions from the real machine. It consist of 4 conductors in each slot, where only the active material, copper, is modelled. All insulators, paper and lacquer on the conductors are modelled as empty space. The conductors are all set as solid conductors in Maxwell, this to be able to show the current distribution and be able to evaluate the current distributions impact on the conductor losses. The hairpin dimensions are 2.5 mm in width and a thickness of 3 mm. In Figure 3.3 one slot is presented.

The hairpin windings is connected in series and excited using a current source. The placement of the conductor in the slot is difficult to model since it is random to some extend. The placement used in this model is motivated in Chapter 5.

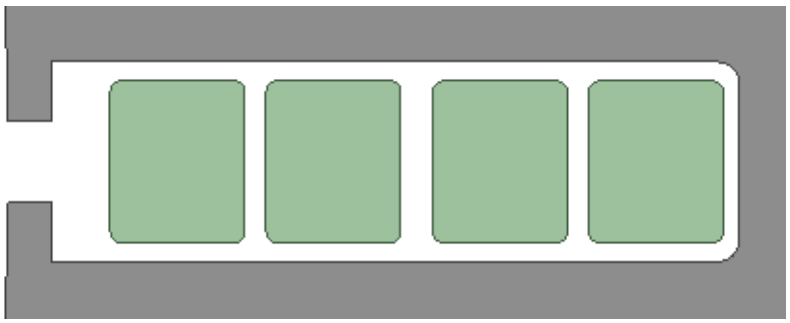

Figure 3.3: One slot of the hairpin winding machine

3.2.3 Sensitivity analysis of hairpin model

Since the FEA depends on how many mesh points and how many calculations that is performed on these points a sensitivity analysis is performed. The number of calculations is quantified by the number of calculations per electric period, further on called steps per period. The analysis aims to minimize simulation time while the results is kept accurate. The study is done by starting with the shortest possible simulation time and then gradually increasing the time by improving the mesh and steps per period separately until a steady state of the quantities under investigation is reached. The quantities examined in the analysis is the conductor losses and torque.

3.2.3.1 Number of Mesh elements

Sensitivity analysis of the mesh is done from the coarsest mesh available in Maxwell giving a total number of elements of 2320 up to a refined mesh containing 29729 elements. The study is performed by simulating the starting mesh and then refinements is made in conductors, stator, stator slots and air gap separately. The refinements is focused in these areas because it is the conductor losses that are the main interest of the report. The results from this test can be seen below in Figure 3.4. From the figure a mesh containing close to 10000 elements is assumed to be enough.

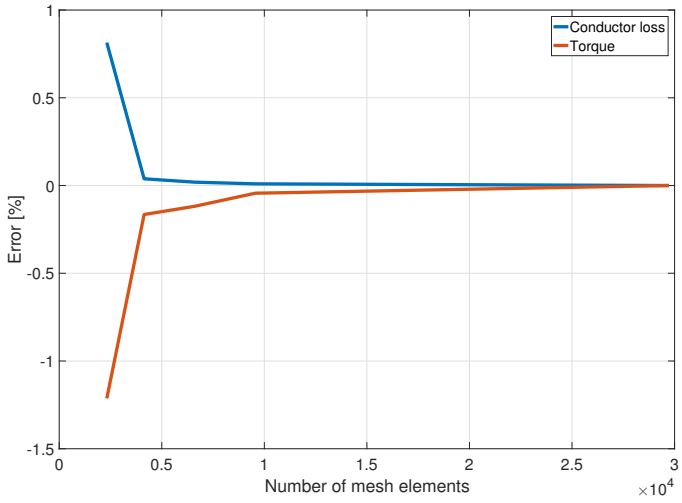

Figure 3.4: Mesh size impact on losses

3.2.3.2 Steps per period

A number of different steps per periods, ranging from 60 to 1580, was simulated. The results, available in figure 3.5, shows that keeping the number of steps above 240 will keep the relative loss towards the most thoroughly case simulated below 0.5%, which is considered to be enough.

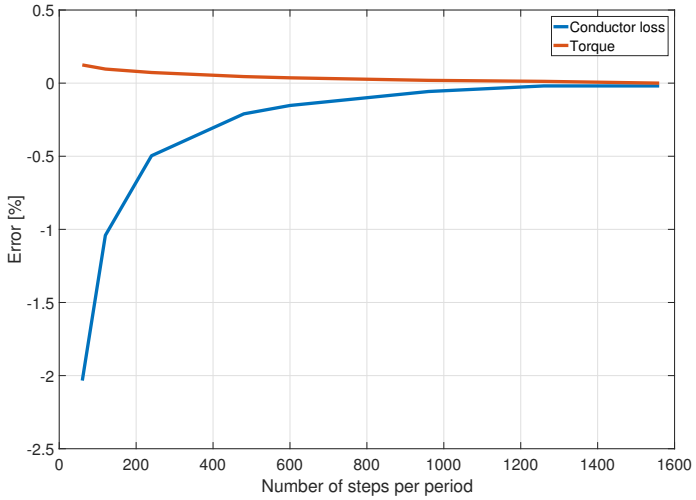

Figure 3.5: Step size impact on losses

3.2.4 Final FEA model of the hairpin winding machine

The final model used for simulations on the hairpin winding is presented in figure 3.6. The conductors is now split in to the three phases, separated by color in the figure. From the figure it is visible that the machine consists of two layers and is short pitched.

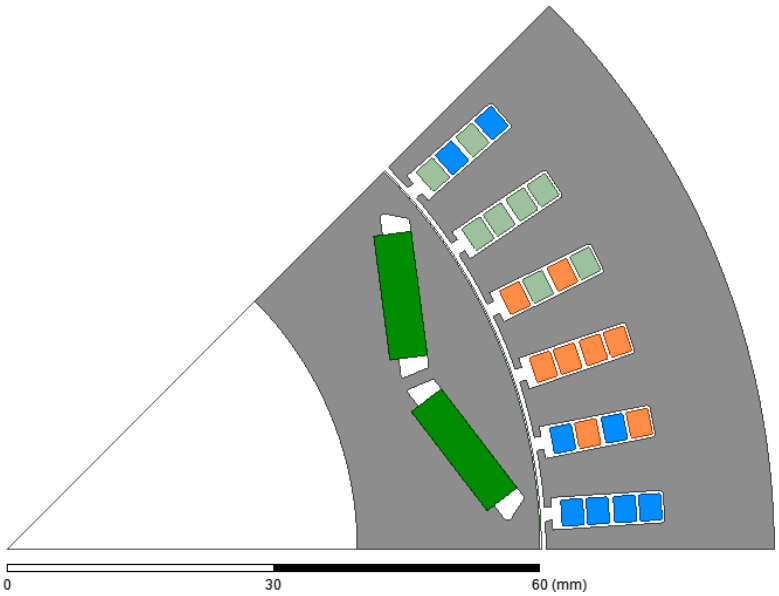

Figure 3.6: Hairpin model used in simulations

The conductors is also named to be able to separate individual conductors. The names is dependent on their position and what phase they belong to. A zoom of phase B presented in Figure 3.7 exemplifies this.

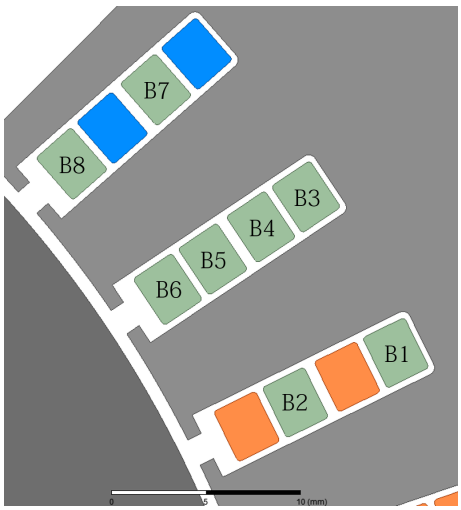

Figure 3.7: Zoomed in version of the hairpin stator with names for individual conductors in phase B

From the sensitivity analysis the steps per period used is 240 and mesh data is presented in 3.2.4.1.

3.2.4.1 Mesh

The number of mesh elements was decided to be 10173 and they are focused on and around the conductors to fully catch all phenomena affecting the losses. The complete mesh can be seen in figure 3.8 and a zoomed in version on one slot and air

gap in figure 3.9. The distribution of the mesh elements are presented with numbers in table 3.5.

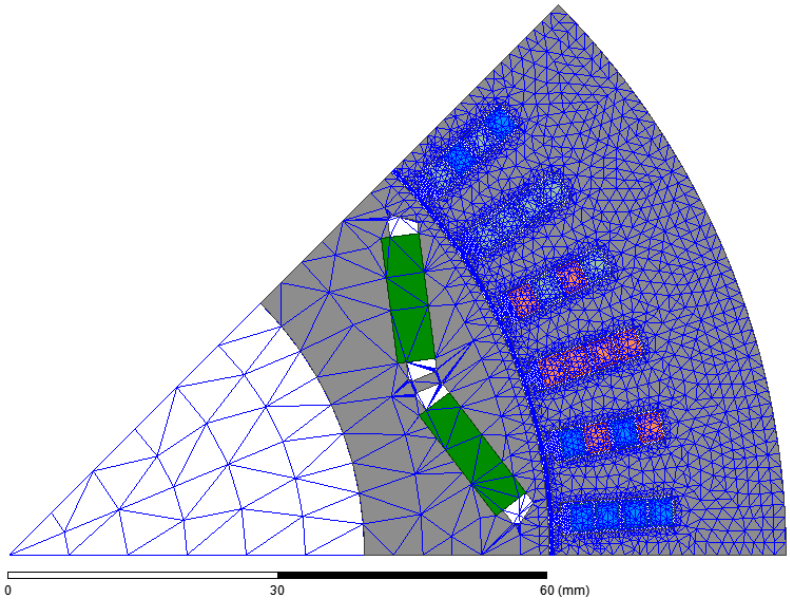

Figure 3.8: Full mesh model

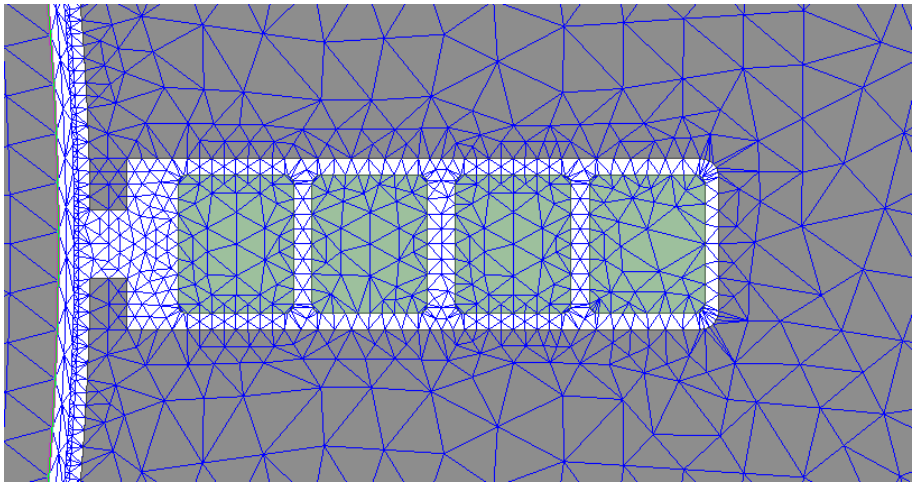

Figure 3.9: Zoomed in mesh model

Table 3.5: Mesh element distribution

Part	Number of elements
Rotor	267
Stator core	3290
Permanent magnets	19
Conductors	84 - 103
Airgap and slot	3973

3.3 FEA model for the random round winding machine

This section will go through the dimension and conductor layout for the model of the random round winding machine. It will also motivate for the number of mesh elements used and also how many steps per period that is used in the simulations.

3.3.1 Motor model for the random round winding machine

As mentioned in the limitations, Section 1.3, the round winding model is not optimised. The reason that it was not optimised is that the purpose of the comparison is to show the behavior of the losses in the round winding, not to compare the total loss of the machine. The key contributor to that the machine is not optimised is that exactly the same stator is used for both the hairpin model and the round winding model. The difference of this approach compared to a more optimised machine is that the stator slot area for the hairpin machine is smaller. Usually the stator slot is designed in a balloon shape as can be seen as the dashed lined in Figure 3.10, compared to the more rectangular shape with rounded edges from the hairpin machine which is also seen in the figure.

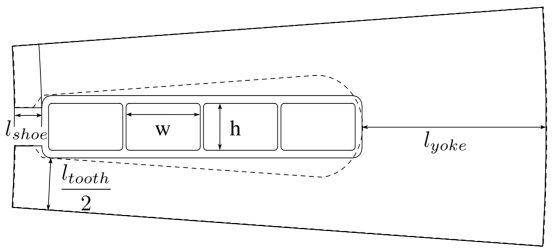

Figure 3.10: Shows a segment of a stator slot in a hairpin machine, the dashed line show an increased slot area for a round winding machine.[2]

According to calculation from the fill factors and total amount of copper presented in the report from [2], the slot area could increase in the range of 35%. Even though the fill factor is lower for a round winding machine, the total amount of copper in the stator windings could be rather high due to a larger slot. The motivation to the decision of not optimising the round motor model is to avoid a discussion of other parameters, such as saturation in iron, iron losses, cooling etc., in a to large extent, which is outside the primary scope of the report. Therefore the same stator and rotor will be used for the two types of winding.

As stated the dimensions for the stator, rotor, stator teeth geometry etc. can be found in section 3.2 and is the same as for the hairpin machine. The difference between the two models is therefore only the windings. The hairpin conductors are deleted and replaced by round windings. The machine model is shown in Figure 3.11 once again only one eight of the machine is modeled due to symmetry and will save time during the later simulations.

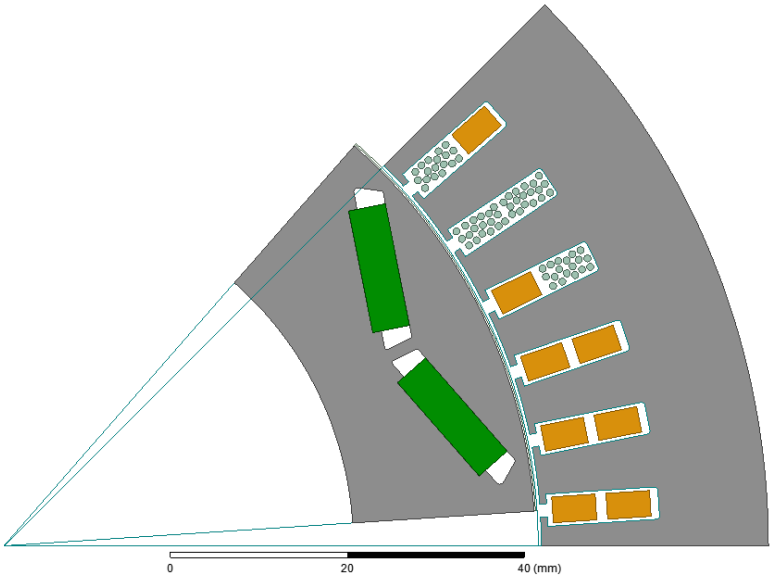

Figure 3.11: Show the geometry of the random round winding machine including windings.

Figure 3.11 also show the windings, it can be seen that only one phase, phase B, is modeled with solid, round copper conductors. The other two phases is modeled with Maxwell's built in conductor blocks to improve the simulation time. The conductor block in Maxwell generate the right amount of flux and back-EMF but ignores additional AC-loss. In the blocks the number of parallel branches has to be set in order to produce the correct flux and back-EMF. The drawback with the conductor block is that it is not able to simulate the current distribution in individual strands nor the copper losses, this is why one phase needs to be modelled with solid conductors. It is enough to simulate only one phase due to symmetry reasons in order to calculate the losses of the full machine.

The number of conductors is decided by setting a typical strand diameter of $0.8mm$ and by using a common fill factor of the round winding machine of 0.4 [2]. Using the slot area and the area of one conductor, 37.6 conductors is calculated to correspond to a fill factor of 0.4. Since this is not an integer it can not be used, instead 36 conductors is used. This is offering some freedom in how the conductors will be divided between phases and number of parallel conductors since it is dividable with both 3 and 2. This allows for changes in back-EMF amplitude and also parallel conductors to allow for higher currents and also for short pitch windings. The true fill factor then becomes 0.383. The result of this conductor setup is shown in Figure 3.12. In the figure it can be seen that there is rather much air in between conductors and walls, this space is reserved for insulation, slot insulation paper and lacquer. Each conductor is surrounded with one layer of insulation of 0.1mm thickness. Around the walls of the slot there is one layer of paper of 0.2mm thickness except in the middle of the slot where there are two layers of paper to separate the different phase layers. Besides these restrictions the conductors are placed freely by hand and a bit random.

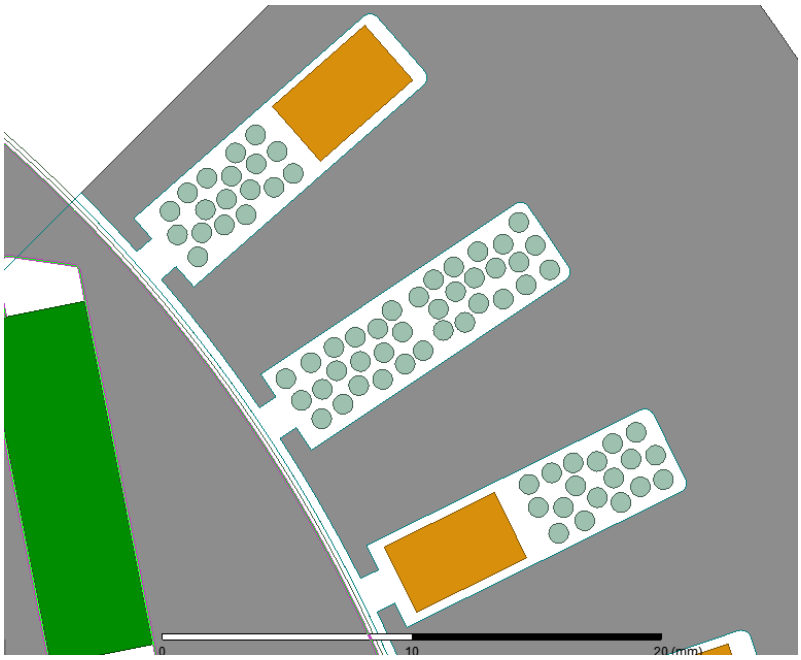

Figure 3.12: Conductor positions in the random round motor model.

3.3.2 External circuit with current source for the random round winding machine

In order for the simulation to run, the round model machine needs an external circuit, shown in Figure 3.13, to be set up to tell Maxwell how the conductors and windings are connected. In the figure the conductors are shown as coils. As mentioned earlier, the conductors has to be split up in order to allow for higher current. The conductors in one slot are split by four into a group of nine parallel conductors, which create a similar setup compared to the hairpin machine but with less copper area due to a lower fill factor. These nine parallel conductors in one group is then series connected with the other groups. This can be seen in the Figure 3.13 as nine parallel conductors and eight series conductors in each parallel branch, note that the series connection is denoted by a dotted line in the figure. As a summation this adds up to 72 conductors in one eighth of the model.

In the model with current source it can be noted that only two current sources is used, or needed. The use of three current sources with Y-connection seems to be limited by the software. However, three current sources is not needed. The use of two current sources can be explained by Kirchoff's Current Law (KCL) where the sum of current in a nodal point is zero. If KCL is applied in the Y-point in Figure 3.13 and if the circuit is balanced, two current sources, shifted 120°, will behave as a set of three current sources shifted 120° between each other in each phase. Therefore this circuit setup will appear exactly as if it was supplied by three identical current sources.

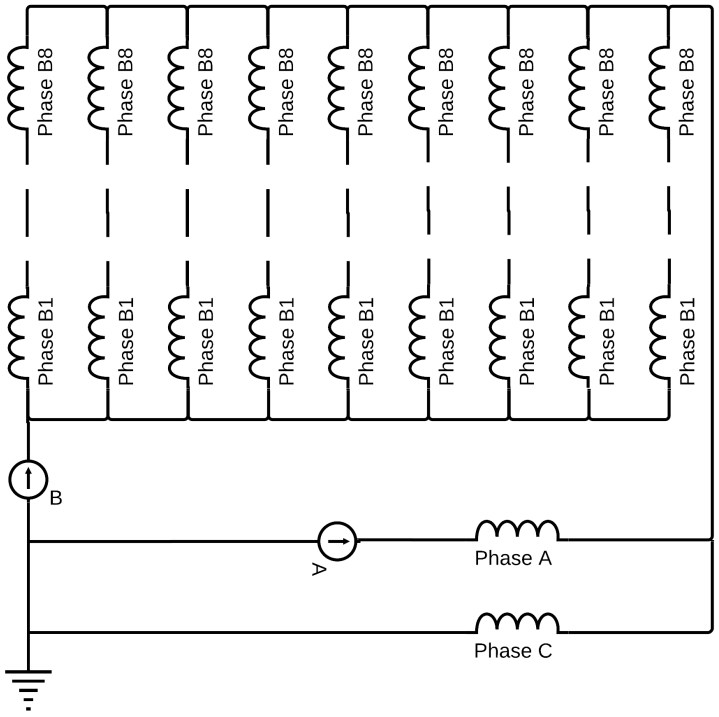

Figure 3.13: The external circuit that is needed to in order to connect the conductors of the machine. Note the series connection denoted by a dotted line consisting of identical circuit components.

3.3.3 Sensitivity analysis of the FEA model for the random round winding machine model

Since the simulation of the machine is done in a FEA model a mesh is needed. In order to save time on calculation a mesh analysis is performed to check how the results of the model is affected by the layout of the mesh and the number of mesh points. Equally important as the mesh is the number of steps per period, which will be examined to see how that influences the results of the simulation, as for the simulation a low number of steps will save time.

3.3.3.1 Mesh analysis for the random round winding machine

In the first round of mesh analysis the focus where on the mesh inside the conductors which is the region of interest for copper losses. The test were performed at 10000rpm, $100A_{rms}$, 144 number of steps per period and made for five different meshes, where the coarsest and finest mesh is shown in Figure 3.14. The number of mesh elements for these meshes are presented in Table 3.6.

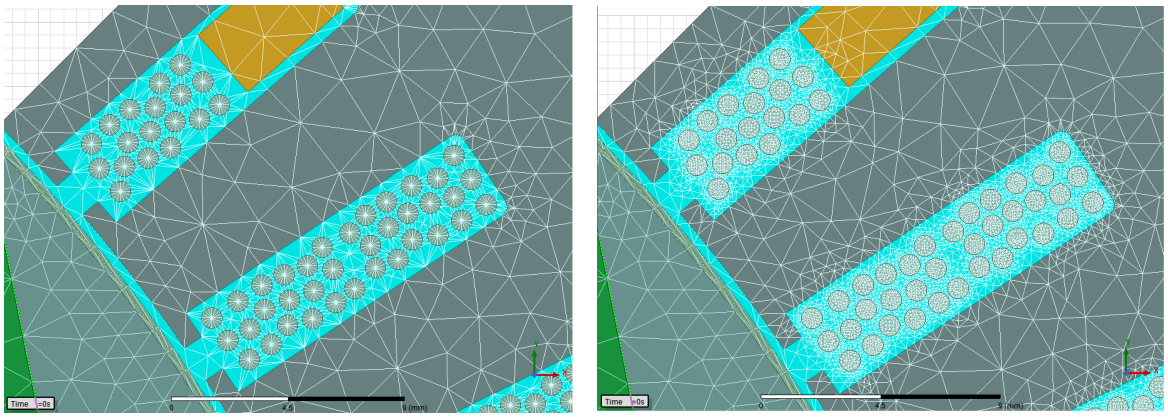

Figure 3.14: The coarsest mesh, Mesh 5, is shown to the left and the finest mesh, Mesh 1, is shown to the right.

Table 3.6: Data of the five tested mesh where Mesh 1 is the finest mesh and Mesh 5 the coarsest.

Number of elements	Mesh 1	Mesh 2	Mesh 3	Mesh 4	Mesh 5
Total	18171	9219	7357	6213	5485
In one conductor	96-112	62-74	40-48	24-28	16-16
Max element size conductor	0.15mm	0.20mm	0.25mm	0.40mm	1mm

The result from the analysis is shown in Figure 3.15 which shows the difference between the results in percentage difference for torque and copper losses, compared to the finest mesh which is set as a reference, since the true value cannot be known. Based on that the difference between the coarsest and finest mesh is less than 0.03% the coarsest mesh is used. It may also be noted that the mesh for the round winding model is less sensitive than the mesh for the hairpin model.

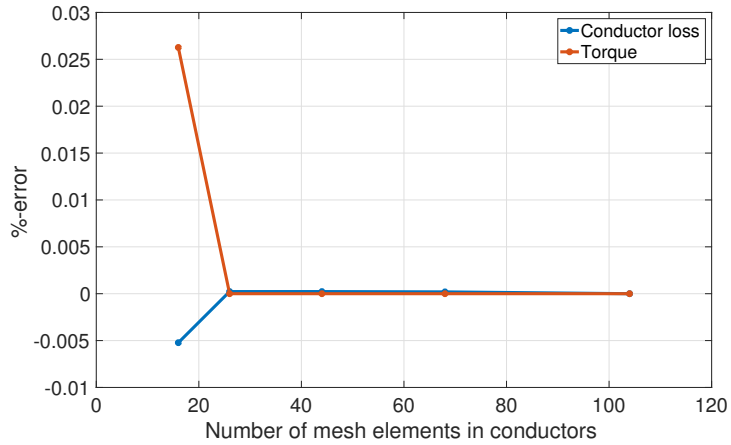

Figure 3.15: Influence of mesh refinements inside conductors.

After the mesh test of mainly the conductors, another mesh test focused on the stator, rotor and air gap was performed to see if this could have any impact on the

result. In this test four different mesh were tested and categorised by the number of elements in the slots, the mesh in the stator for this test were the same for the different mesh test and same as the final stator mesh in the hairpin stator. The final mesh for the random round winding is shown in Figure 3.16 and the data for the mesh are presented in Table 3.7.

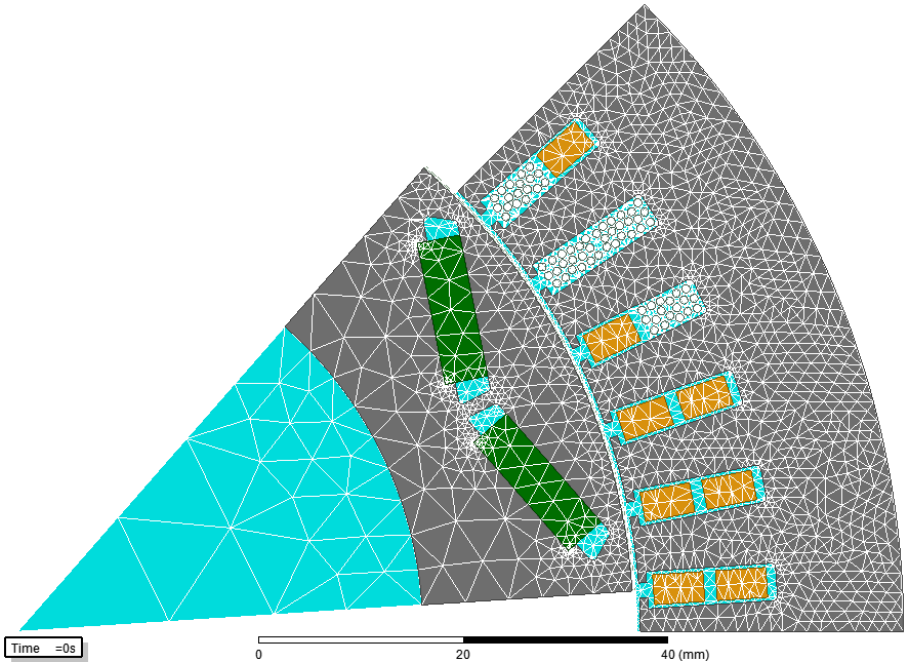

Figure 3.16: shows the final mesh for the round winding model

Table 3.7: Shows data for the mesh refinements in stator, rotor and the four different mesh refinements in air gap.

Number of elements	Mesh 1	Mesh 2	Mesh 3	Mesh 4
Total	10792	7912	7341	6816
In air gap	4001	2502	2266	2030
Max element size air gap	0.5mm	0.8mm	1mm	1.5mm

In this test the speed and current where the same but 240 number of steps per period was used. The result of the test for torque and copper loss is presented in Figure 3.17. From these results the coarsest mesh is used to shorten the simulation time and since the deviation is small, less than 0.14%. The final mesh was then also compared with the same mesh but refined in the conductors with no large difference.

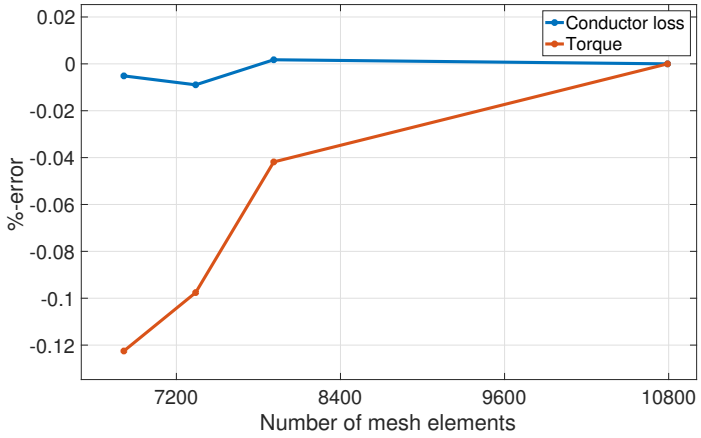

Figure 3.17: Influence of mesh refinements around in stator, rotor and air gap.

Finally the data for the mesh for all parts of the final model used in the simulations are presented in Table 3.8.

Table 3.8: Mesh element distribution

Part	Number of elements
Rotor	790
Stator core	2065
Permanent magnets	71
Conductors	16
Airgap and slot	2030
Conductor blocks	19-28

3.3.3.2 Number of steps per period analysis for the random round winding machine model

For the final mesh a number of steps per period test were performed in order to analyse how the torque and copper loss was influenced. The results of the step test is shown in Figure 3.18, from these results 240 steps/period is used since the deviation is less than 0.2%. In one additional test for the chosen speed 240 steps/period a finer mesh were tested with no great influence. Therefore the number of steps per period used for the simulations is 240.

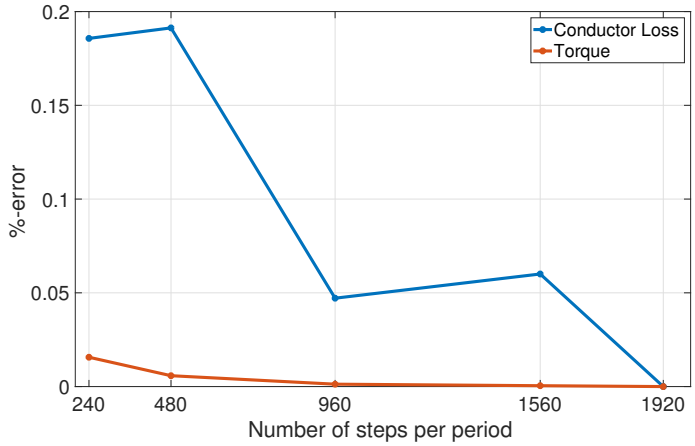

Figure 3.18: Impact of number of steps per period for torque and copper loss.

4
Simulation

This chapter presents the setup and result of the simulations performed. First of all the simulation of the full hairpin machine is presented, including a study of number of layers and stator slot opening, then a comparison of the hairpin and round random winding machine regarding copper losses and resistance is presented. For the hairpin machine, coupling to physical phenomena will be made regarding eddy effects. Throughout the chapter analytical results are also presented and compared to results from the FEA.

4.1 Simulation setup

For all simulation setups the different measurement points is excited using a current source. The drawback with this is the absence of harmonics in the current but the advantage is that it allows for quicker simulations. Since a current source is used and the nominal current is not available in data sheet the applied current used is an approximated *nominal current* of $88A_{rms}$. This is verified by that the model develops a torque a couple of percentage over the nominal torque of 70 Nm. Since rotor skewing is not used in our model this current is considered to be good enough. The *nominal current* is then used over the whole operating range of 0-10000 rpm, since field weakening not is considered.

To make sure that points are comparable all currents are simulated on the MTPA angle, which is calculated by Ansys Maxwell. The maximum speed of the machine is 10000 rpm which corresponds to a frequency of 666.66 Hz. The full machine tests are simulated between 1 - 2000 Hz, this to get a more general understanding of copper losses, even at speed outside the machine operating range. Lastly, as presented earlier only the active part of the machine is simulated. End windings would affect the results but since this is a 2D simulation only different approximations of the impact of end windings is possible, due to this only the active part is considered.

4.2 Hairpin machine copper losses

The total copper losses in the active part of the hairpin machine is presented in Figure 4.1. The machine is simulated from a frequency of 1 Hz, which gives a Uniform Current Distribution (*UCD*) in the conductors, which also represent the DC case when calculating Rac/Rdc, up to a frequency of 2000 Hz with a sinusoidal current source at $88A_{rms}$.

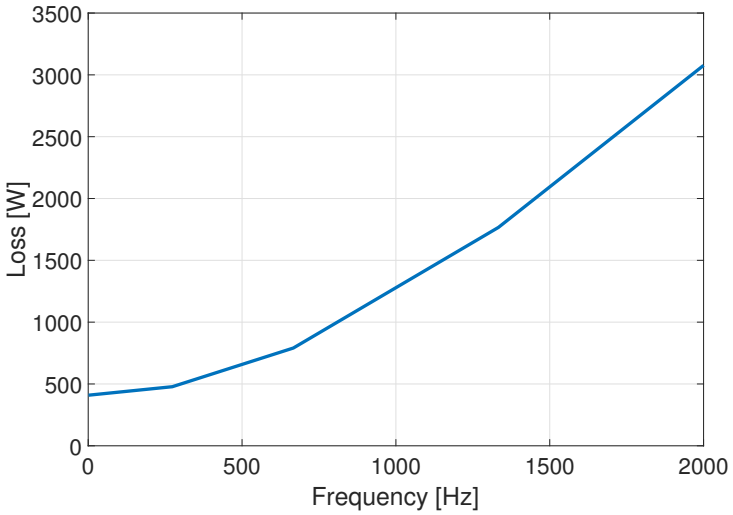

Figure 4.1: Total copper loss in active part of the machine

From these losses the total resistance in the active part can be calculated. The increase in the resistance is presented in Figure 4.2 where the impact on resistance is plotted as the quota of AC resistance to DC resistance. Since the DC resistance is constant, the increase in resistance is due to AC effects. At the starting point being a low frequency, 1 Hz, no AC effect are present and the quota is unity.

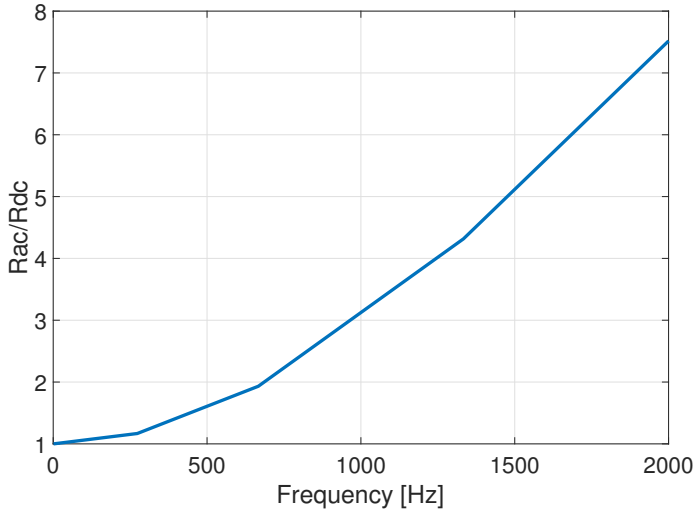

Figure 4.2: AC/DC ratio of the resistance in the active part of the machine

This increase in resistance is caused by redistribution of current density in the conductors. The redistribution of current density is causing a crowding effect of current and the current flowing through the conductors has a smaller area to flow through, causing a higher resistance. In Figure 4.3 the distribution of current is shown for different frequencies at two time instances, peak current and zero current, in the four conductors placed in a slot consisting of only phase B. The figures are gathered when running the motor at speeds, 1 Hz which representing the case with

no AC affects, 273.33 Hz which represents the base speed of 4100 rpm and 666.666 Hz representing the maximum speed of 10000 rpm.

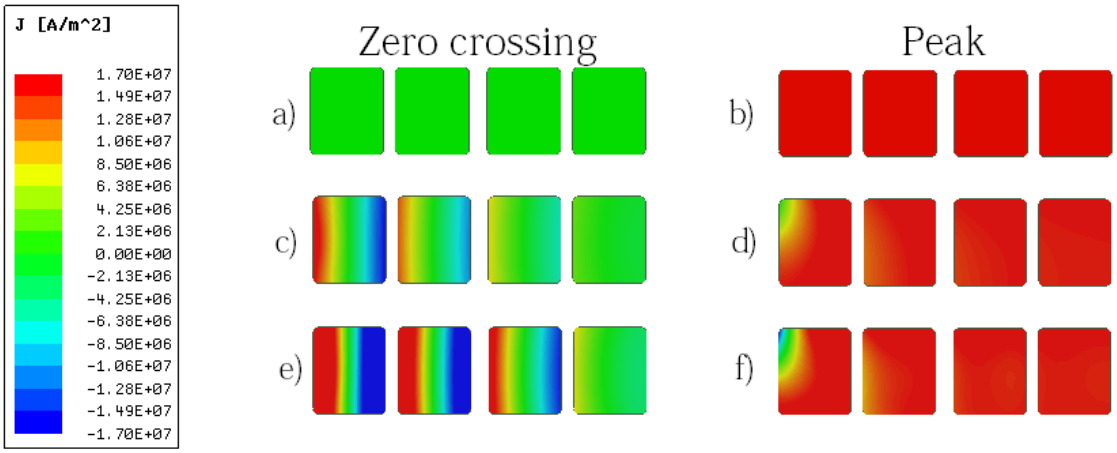

Figure 4.3: Current density for different frequencies at two different time instances with rotor placed to the left of the conductors. 1 Hz (low speed) in (a) and (b), 273.33 Hz (nominal speed) for (c) and (d) and 666.67 Hz (max speed) for (e) and (f).

From Section 2.6.1.1 it is shown that the induced eddy effect are largest when the change of flux is largest. Since flux is proportional to the current the change of flux is largest when the current is crossing zero. Therefore, Figure 4.3 show that there are more redistribution of currents at the zero crossing than at max current.

Figure 4.3 also show that for low frequencies, a and b, the current distributions are uniform. If the frequencies are increased, c-f, the current gets more redistributed, the higher the frequency get. In addition the figure shows that the conductors closer to the rotor are more affected, the reason for this is further investigated later in the thesis.

In the top left corners of the peak current figures, (b), (d) and (f) a change in currents distribution is visible. This change is happening here due to the rotational direction of the rotor and is caused by flux that is passing through the slot in the conductor closest to the rotor. It is later shown, in this chapter, that the flux is being pushed around the slot and due to the load angle the flux is cutting corners through the slot.

To further show how the resistance and thus the corresponding losses are affected, the total loss in one conductor is collected. This is done by integrating the ohmic loss over the surface of a conductor and then scale it with the active length. As shown before in Figure 4.3 the effect is most evident in the conductors closest to rotor. Therefore, in Figure 4.4, the total losses according to (2.12) over one electrical period is presented for the conductor closest to the rotor.

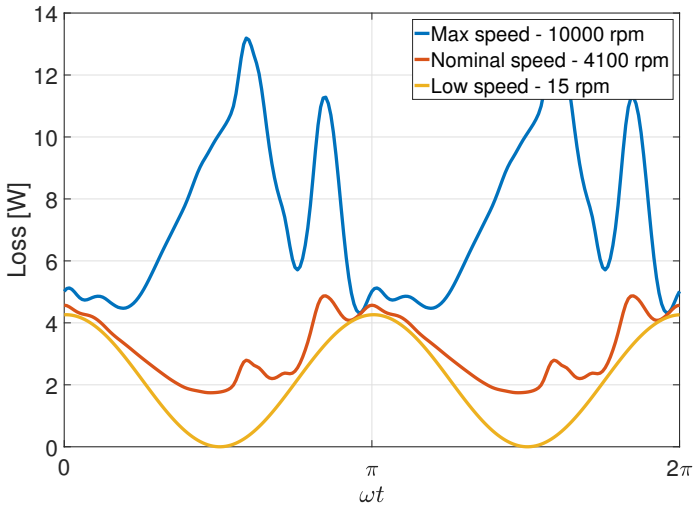

Figure 4.4: Ohmic loss of the conductor closest to the rotor, B6, plotted over one period and at three different speed.

This now shows the total loss in the conductors. In order to observe only the additional AC-loss, the loss contribution from the *UCD* is subtracted from the total loss in Figure 4.4. The additional AC-loss is plotted in Figure 4.5.

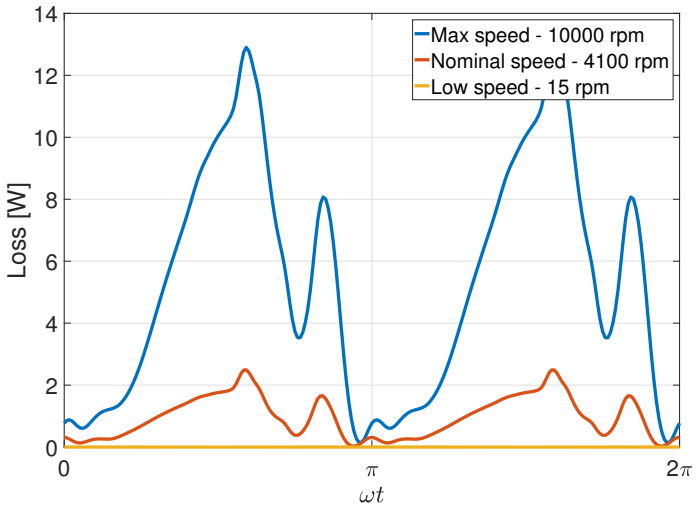

Figure 4.5: AC loss over one electrical period. Loss in low speed case is unaffected by AC affects therefore it is zero.

Now it could be seen that the additional loss is lowest when the net current is at its maximum at $\omega t = n\pi$, where $n = \pm 0, 1, 2, 4, ...$ This since as discussed earlier the rate of change in flux is causing the induced EMF and at peak current the rate of change is zero, while at a zero crossing ($\omega t = n\pi/2$, where $n = \pm 1, 3, 5, ..$) the rate of change is maximum. The figure also show that the AC effect caused losses are speed dependent and contains two distinct peaks.

In the machine all increase in resistance will be evenly spread out between poles and phases due to symmetry. Until now one slot, containing only the B phase, has been shown and as previously mentioned the conductor location in the slot appears to affect the magnitude of current redistribution. So, if looking at one pole of phase B, consisting of eight conductors, the resistance varies. By averaging the loss in each conductor over one period the resistance of that conductor can be calculated. In Figure 4.6 the resistance divided by the *UCD* resistance is presented for each conductor in one pole of the B phase. The *UCD* resistance represent the resistance with no AC effect present. The figure show once more that conductors closer to the rotor is more exposed to effects increasing its resistance. The placement of the conductors can be seen in Figure 3.7.

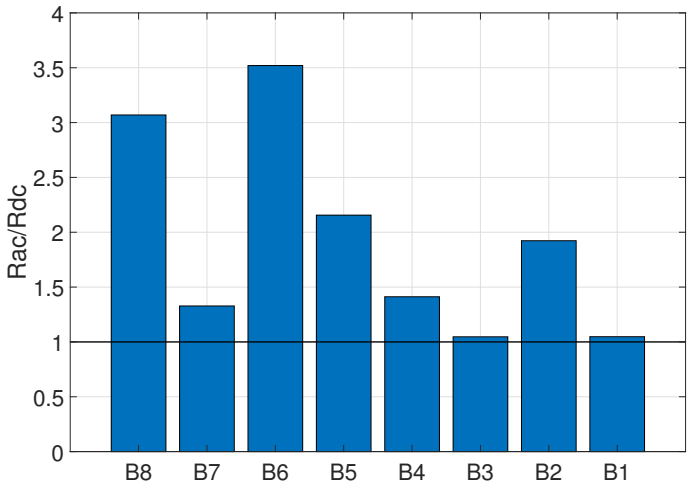

Figure 4.6: Resistance quota per conductor in phase B with the *UCD* resistance as DC resistance.

So, the majority of the losses in one slot is developed in the conductor closest to the rotor. In Figure 4.7 the distribution of losses between conductors in one slot toward speed is shown. At low speed, the losses are evenly distributed, with 25% per conductor, but with increasing speed the distribution of loss in the conductors are changing. At maximum speed The conductor closest to rotor develops 43% of the losses, keep in mind also that the total losses now i twice the total loss in low speed case.

As presented earlier the machine is short pitched which makes half of the slots carrying a single phase while the other half are carrying mixed phases. The distribution of losses is similar in the mixed slots, although the total loss is lower, which will be further presented in the following chapters.

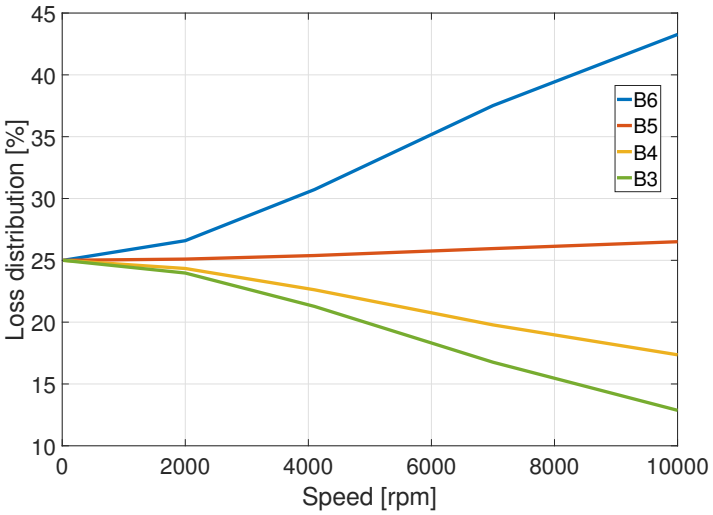

Figure 4.7: Loss per conductor in one slot over full operating range.

4.2.1 Source of additional losses in the stator winding

To examine what phenomenons is causing the resistance to increase, leading to higher losses, the motor model is broken down into parts and simulated. All tests are performed at the maximum speed of the machine, 10000 rpm or 666.667 Hz and at the estimated *nominal current*, $88A_{rms}$, This, since the increase of resistance is significant at this point, while keeping within operating range for the machine under investigation.

4.2.1.1 Simplified eddy effects

To start the analysis of the additional resistance, four conductors representing the number of conductors in one slot, are placed in free space with a sinusoidal current source applied. Then, to examine the influence of conductors surrounded by iron the conductors are placed in an iron bar, with equally much iron on all sides. Finally the iron bar is formed in to a slot segment from the real stator. The setups are presented in Figures 4.8 and 4.9. The placement of the conductors are the same for all setups, B6 to the left and B3 to the right.

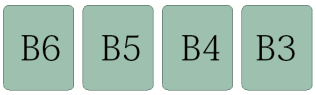

Figure 4.8: Four conductors placed in free space. The names indicate phase and placement, see Figure 4.16

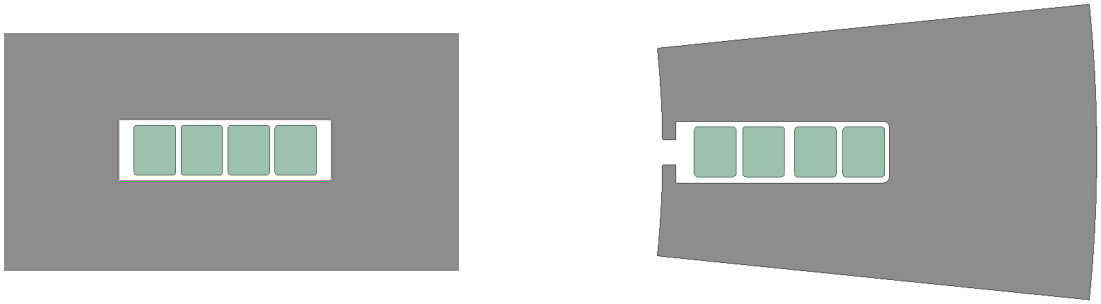

Figure 4.9: Conductors placed in a piece of iron to the left and conductors placed in one slot segment from the full stator to the right.

The resulting resistance quota in each conductor is presented in Figure 4.10 with the *UCD* resistance in a conductor as a reference. The increase in resistance between the *UCD* resistance and conductor resistance is caused by the proximity effect between conductors.

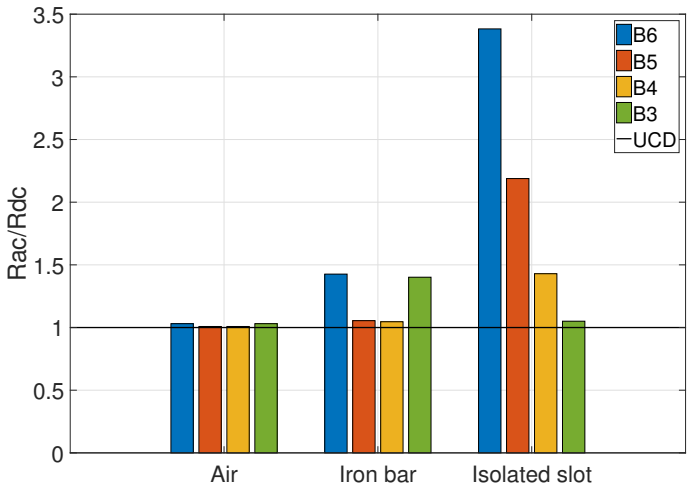

Figure 4.10: Resistance in each conductor for the three different setups. The UCD line indicate the resistance with no AC effects.

For the two symmetric cases in the figure, Air and Iron bar, conductors B4, B5 and B3, B6 has equal change in resistance due to the symmetry of the geometry. For the case with conductors surrounded by air the flux is going to be generated according to the right hand rule which is causing a slight increase in resistance in conductor B6 and B3.

As for the case with an Iron bar the flux will be generated in the same way again but this time the majority will go inside the iron since it offers a path with lower reluctance than the air. Similar to a parallel connection where the current is divided according to the resistance some flux will pass through the conductors since it also offers a way for the flux. This flux is called *leakage flux* and the impact of this can be seen in the resistance increase in conductors B6 and B3 in the Iron bar setup.

In the Isolated slot setup the iron bar is modified to have an air gap on one side of the conductors. This increases the reluctance and more flux is going the alternative way through the conductors. This increase in leakage flux is causing the increase of resistance in the conductors closer to the slot opening. In Figure 4.11 this is shown by presenting the flux lines for the Iron bar and Isolated slot setup at peak current.

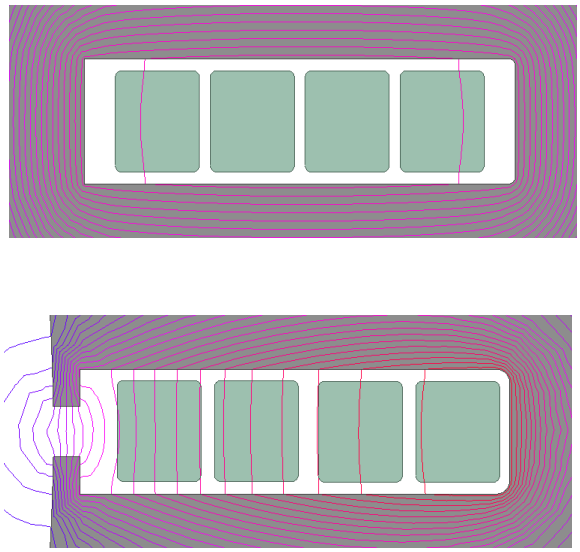

Figure 4.11: Flux lines for the two setup with Iron bar on top and Isolated slot on bottom at peak current

So, when the conductors are placed in the slot segment the resistance gets higher towards the slot opening, due to higher flux leakage. Since the resistance is calculated from the losses in the conductors, and to further examine what is happening in the isolated slot case, the loss over one period in the active part of all four conductors are presented in figure 4.12. The loss from the *UCD* is added as a reference.

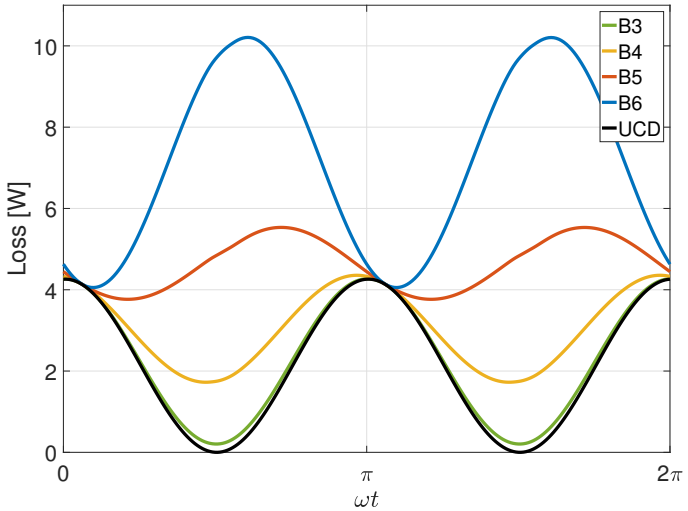

Figure 4.12: The total loss in each conductor in an isolated slot segment over one period. The black line represents the UCD loss in a conductor.

Figure 4.12 shows the total loss in the conductors. To be able to examine only the AC loss the *UCD* losses is subtracted from the total loss. This leaves the loss only from AC effect, presented in Figure 4.13, again with the *UCD* loss as reference.

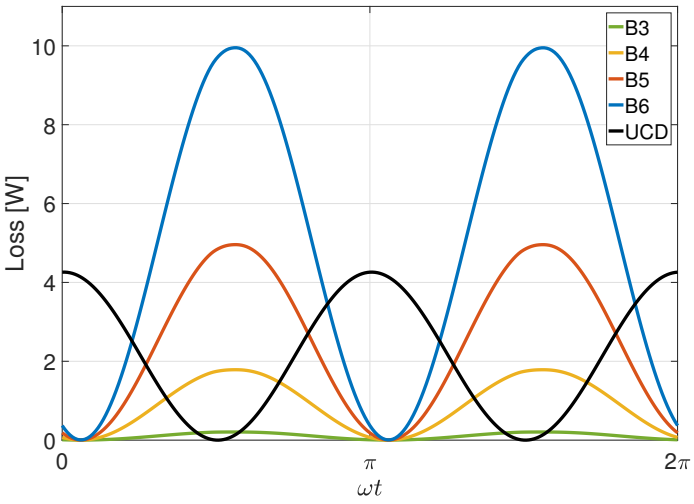

Figure 4.13: Pure AC Loss in each conductor over one period. The pure DC loss in a conductor as reference

Now it is easier to see that the induced AC loss is most significant when the current is crossing zero. In this case no other effects are present except the pure proximity of the conductors them self. The peak in loss occurs with a small time delay from the zero crossing in the current. This time delay is due to the inductance in the conductors.

To validate our model and simulations an analytical approach is considered. The analytical calculations only considers an isolated slot segment similar to the one simulated here. The result from analytical calculations is presented as resistance quotas per conductors over the full operating range in Figure 4.14

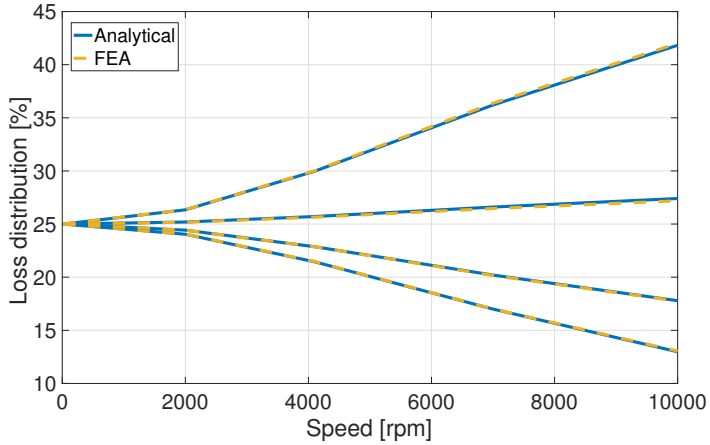

Figure 4.14: Analytical calculations of distribution of losses compared to results from FEA study. B6 on top, B5, B4 and finally B3 on bottom.

This distribution shows that the analytical calculations are close to FEA results over the whole operating range. If now comparing analytical calculations with FEA at the worst point, 10000 rpm, the difference is below 1% which is presented in Figure 4.15.

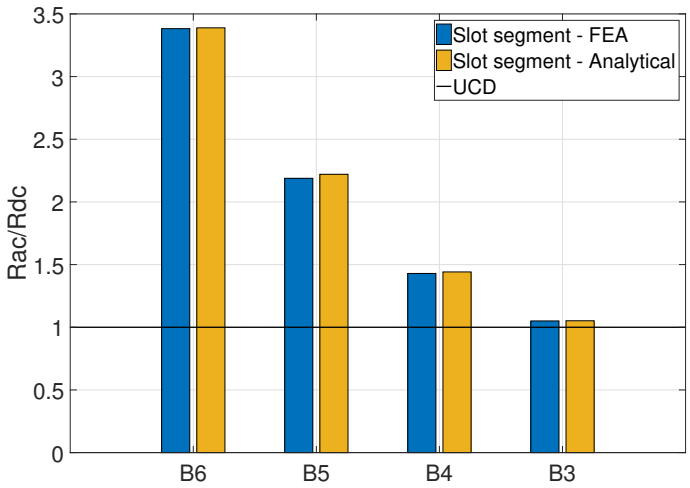

Figure 4.15: Comparison between analytical calculation and FEA at 10000rpm.

4.2.1.2 Eddy effects in the full motor model

Now the isolated slot segment is replaced with the full model of one pole. A pure iron rotor is added to isolate the stator from any effects from the original rotor. The setups is presented in Figure 4.16 where the colors indicate what phase it belongs to and the numbering referring to its position. Where green is phase B, orange phase C and blue phase A.

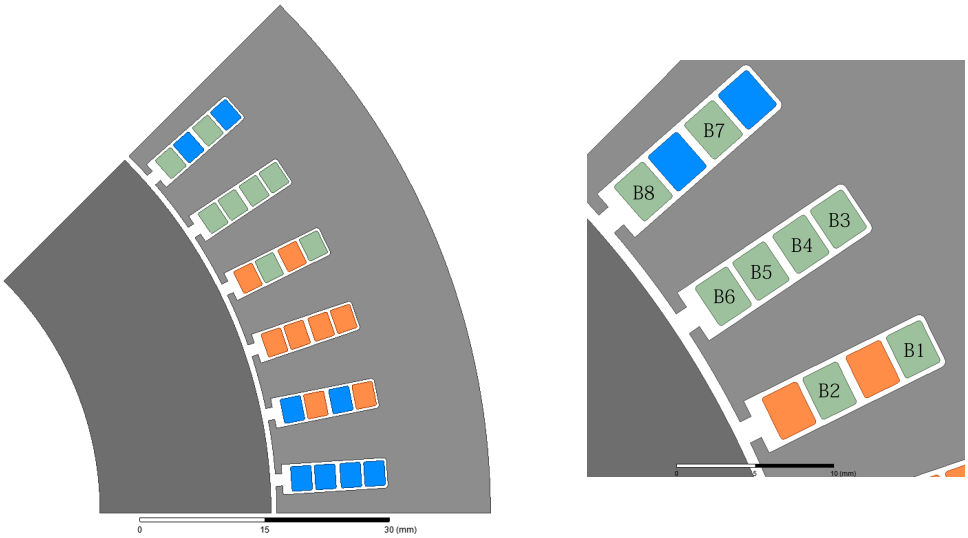

Figure 4.16: Setup for one pole of the machine with a pure iron rotor showing the three phases in different colors and the numbering of conductors

The first test focuses on the conductors in the slot with only phase B, this to be able to compare with the isolated slot segment test. So, the impact the additional conductors B1-B2 and B7-B8 have on the resistance in B3-B6 is investigated. This is done by applying zero current on phases A and C and the *nominal current* on phase B. After this the same current amplitude but with a ±120 degree shift is applied to phases A and C. As described earlier the current in one phase next to another phase is applied in the opposite direction to create the rotating flux vector. The resulting resistance quotas can be seen in Figure 4.17.

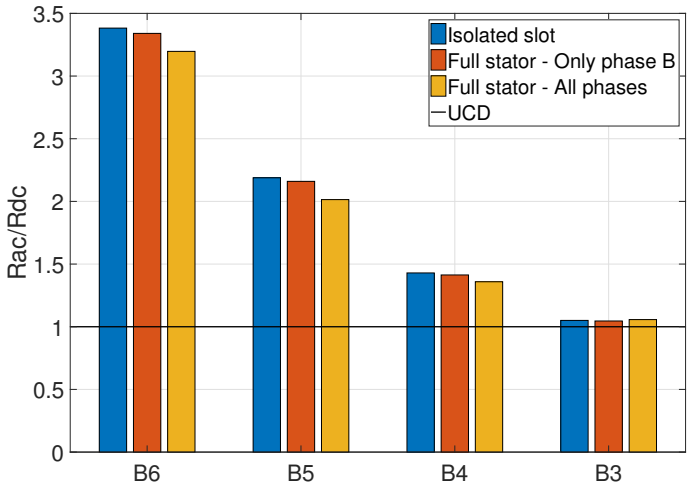

Figure 4.17: The total loss in each conductor for different setups. *UCD* is added as reference.

The figure 4.17 shows that the resistance is decreasing when applying current in the extra phase B conductors. Also when applying current in phases A and C the resistance decreases. This is due to that less leakage flux is passing through the slot. So the conductors outside the slot has given the flux alternative ways to go. The difference in the way the flux chooses, between the setup with only phase B current and the setup with current in all phases, can be seen in Figure 4.18.

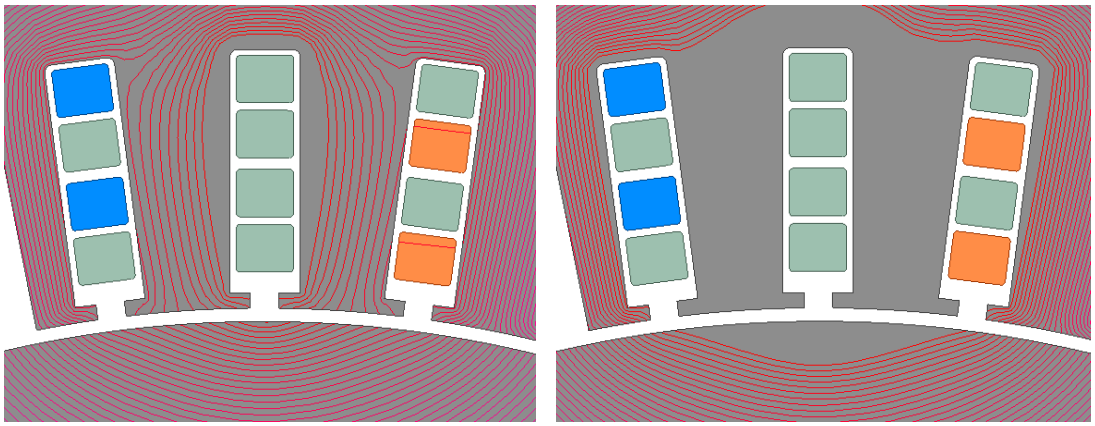

Figure 4.18: Flux lines for the cases with current only in phase B (green conductors) to the left and current in all phases to the right.

The figure shows that when applying current in all phases the flux is pushed out from the middle slot, creating a gap of lower flux. This gap is decreasing the leakage flux and thus the resistance. Note that the figures show areas of no flux but there is flux everywhere, these figures are just scaled to the same range of flux amplitude to clearly show the phenomena.

Earlier the loss in the conductor had its peak when the current was at a zero crossing. In this case when the flux has been pushed out from the slot the peak in loss has shifted. Figure 4.19, where the pure AC loss in conductor, B6, is presented, show a drop in the loss where the peak happen earlier, instead the edges has grown larger indicating that the change of flux is now largest before and after the zero crossing in current. This is due to that the conductors that are on the edges of the low flux gap would experience a high change of flux while the conductors in the middle would experience a more constant flux. As presented earlier the loss in B3-B5 shows the same, but scaled down, behaviour as B6 therefore only the loss in B6 is presented with the *UCD* loss as reference.

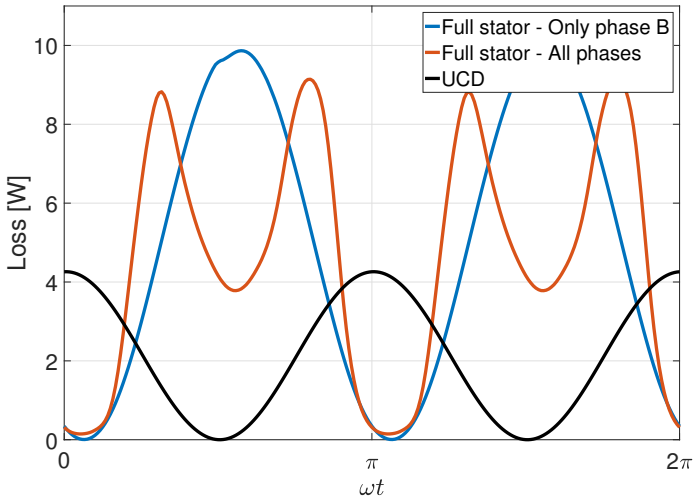

Figure 4.19: The total AC loss in B6 for the two cases with current in phase B and current in all phases. *UCD* loss is added as reference.

Now, also the other conductors of phase B is added and the resulting resistance quotas is presented in 4.20.

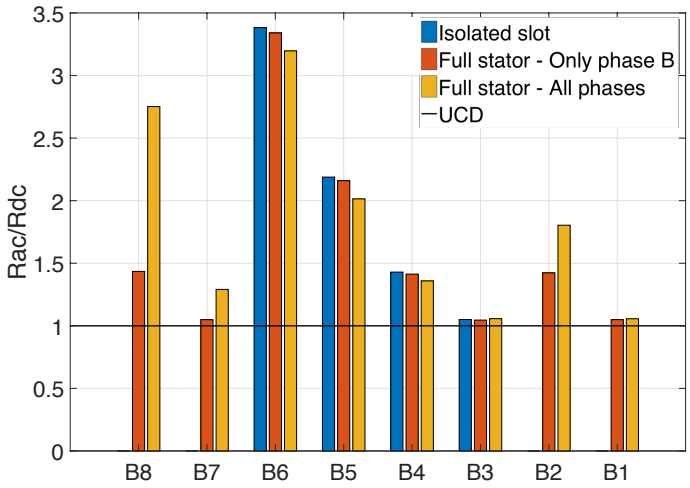

Figure 4.20: The total loss in each conductor. The result for conductors B3-B6 is the same as the previous plot.

If now focusing on the red bars where current only goes in the phase B conductors the conductor placement relative to one another appear to play a big part in deciding the resistances. To make it clearer, Figure 4.21 show the conductor placement again.

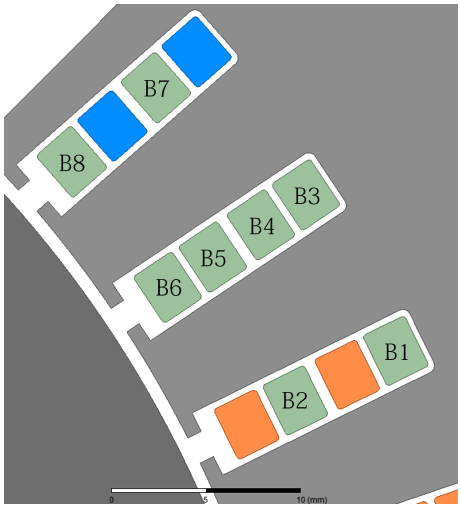

Figure 4.21: One segment of the stator with full phase B shown

B1, B3 and B7 will all be the conductor closest to the yoke and the resistance in these are all the same. In this case, with current only in phase B, the conductors B2, B4 and B8 are all placed with only one current carrying conductor between them and the yoke. The leakage flux through these appears to be the same since the resistance in these are close to each other. The difference in resistance is presented in Figure 4.22 with the lowest resistance, B4 as reference.

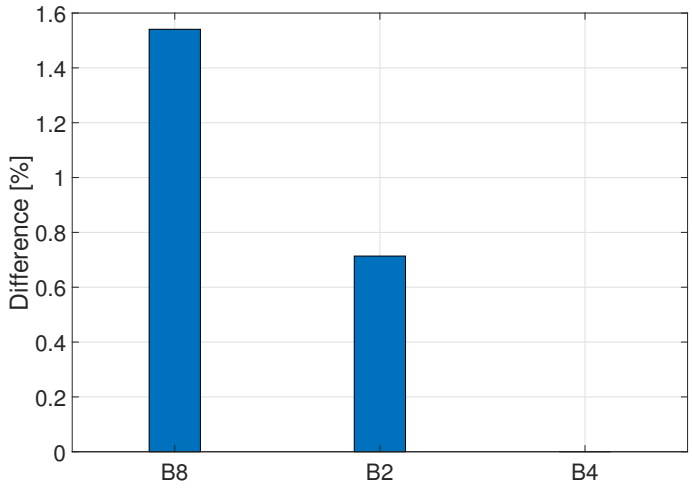

Figure 4.22: The relative difference in resistance between conductors

This relative small difference would imply that the distance to the slot opening and the number of current carrying conductor between the conductor and the slot opening plays a small role if the current in the conductors between the conductor and the stator yoke is the same.

If now instead looking at the yellow bars representing the case with current in all phases, they show that the loss in B8 and B6 differs. This is explained by that the current in phase A, which the blue conductors are carrying, are leading phase B current by 120 degrees. But, as explained earlier, since phase A in this position is in the opposite direction it instead lags 60 degrees. This means that the flux induced by this slot would not be in phase with the slot containing only phase B. Instead the flux induced from this mixed slot will be a combination of the flux from phase B and phase A. This gives a delay in flux peak by 30 degrees which is visible in the losses, this lag between fluxes also lowers the peak flux causing lower induced losses. This delay and decrease in loss can be seen in Figure 4.23 that presents the loss in conductors B6 and B8, two conductors in the same position in their respective slots.

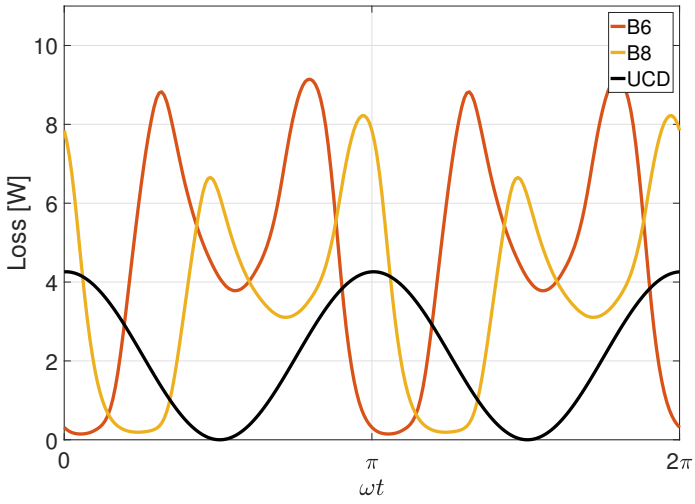

Figure 4.23: The loss in conductors B6 and B8 over one electric period. The UCD loss for a phase B conductor is added as reference.

This again show that the loss in the conductors rely on the current in the conductors between them and the yoke. So to conclude, with a rotor of pure iron the placement within the slots is less important compared to how many and what phase the current carrying conductors that are placed between the conductor and the yoke are.

4.2.1.3 Reluctance and magnet rotor

Now the impact of adding a space for the magnets in the rotor, called reluctance rotor, is considered. This is changing the reluctance in the rotor and how this affect the resistance in the conductors is investigated. Lastly the magnets is added to see the final result. Figure 4.24 presents the two setups.

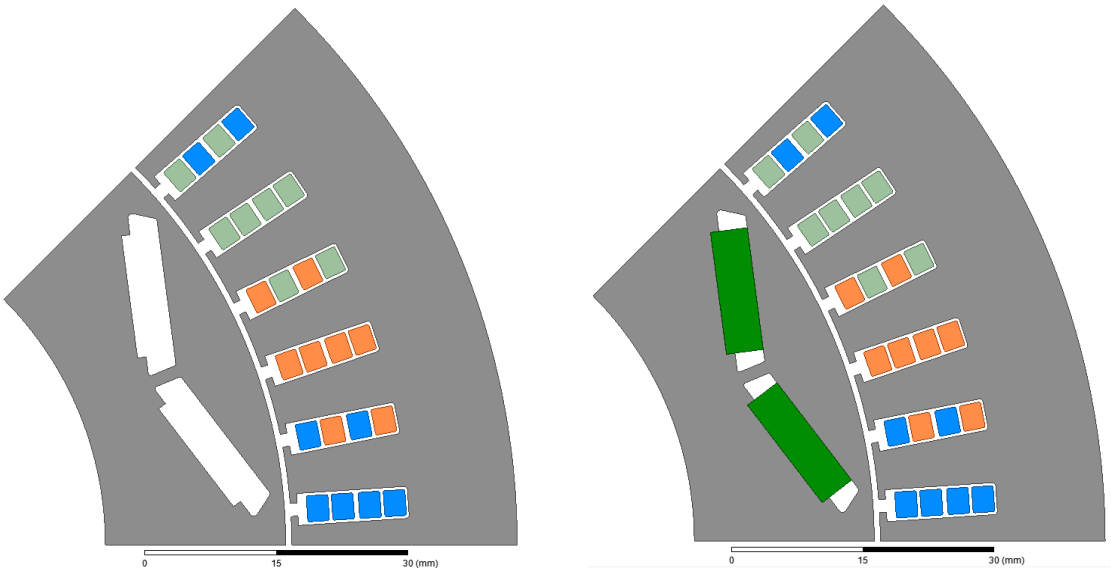

Figure 4.24: Setup for full machine without magnets to the left and with magnets to the right.

First, in figure 4.25 the impact of the rotor with air gaps is shown. It is implemented with no current angle meaning that no torque is developed. It can be seen that the flux still gets pushed out from the teeth surrounding the slots with highest current. And since the air gaps now are symmetrically placed the only difference is that it gets a little bit more concentrated in the rotor to avoid going through the high reluctance air spaces.

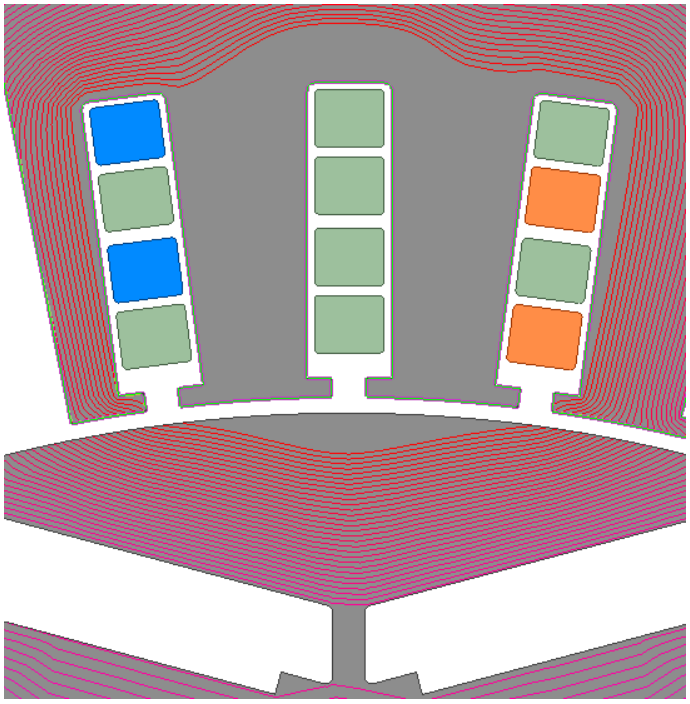

Figure 4.25: Flux line distribution when adding rotor with air gaps for magnets and no current angle applied.

If now beginning to apply the current angle, which causes the machine to start develop torque, the flux will be re-distributed to handle that the reluctance paths no longer is symmetrical around the slot carrying the highest current. This current angle will cause the rotor to lag, mechanical angle equals current angle divided by pole pairs, thus causing the V-shaped air gaps to lag the peak current slots. The impact of this change in current angle is presented in figure 4.26 which presents the flux distributions for the current angles 10 and 35 degrees. The last point is at 35 degrees because it is the calculated MTPA angle for the full machine. With this being a machine with four pole pairs the mechanical angle lag is at most 8.75 degrees.

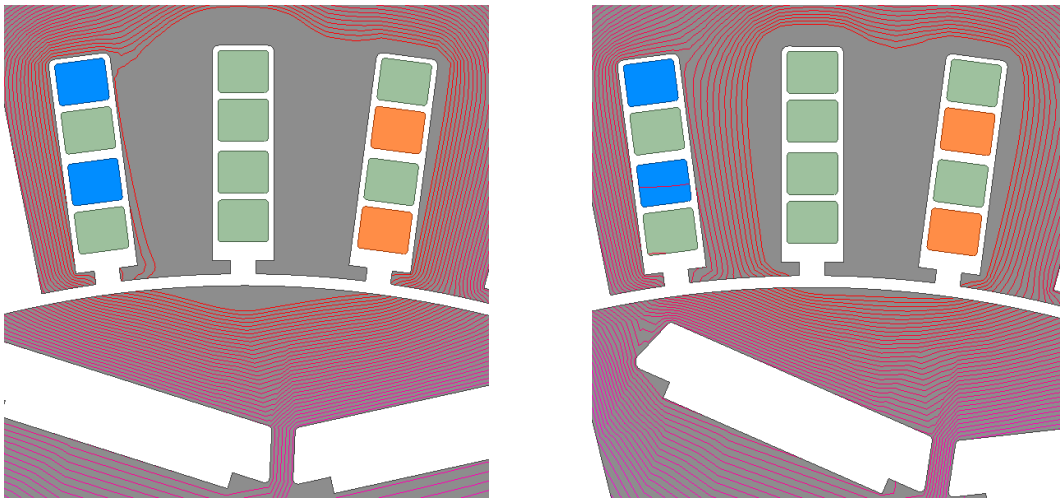

Figure 4.26: Flux lines for two different current angles, 10 degrees to the left and 35 degrees to the right.

So, the flux lines still follows the least reluctance path in the rotor causing the gap in flux, which was earlier seen in the teeth surrounding the peak current slots, to shift. This shift will change the losses in the conductors and how the AC loss in conductor B6 gets affected for a number of different angles can be seen in figure 4.27.

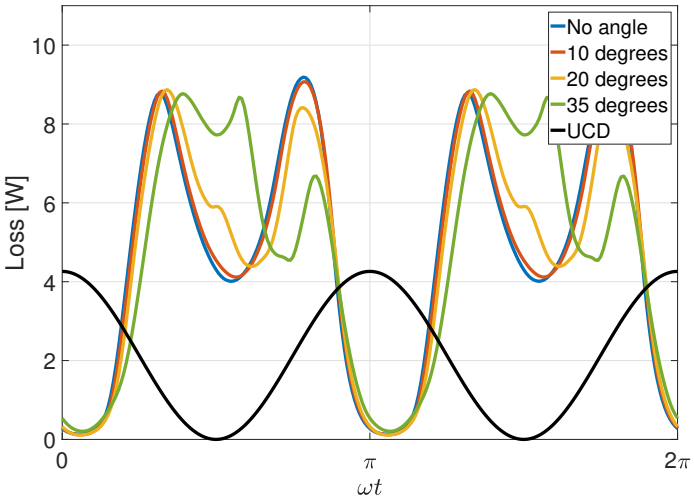

Figure 4.27: Impact of current angle on the AC loss in conductor B6

As discussed earlier in the thesis the behaviour in the other conductors are either shifted in time or shifted in magnitude, thus the losses in B6 is considered to contain all information.

Lastly, the same approach is used for when the magnets are attached, starting with no current angle and increasing until MTPA angle. Since the magnets now is contributing with flux on their own this flux will coincide with the flux from the stator conductors. At peak current in phase B the current is going in to the plane

and thus creating a flux, according to the right hand rule, that pushes the magnets flux to the left. When the current angle is increased this push is not managing to push all the magnet flux leading to more flux crossing through the previously flux free teeth and also the conductors. In Figure 4.28 the comparison in flux line distribution of no angle and 10 degree angle is shown.

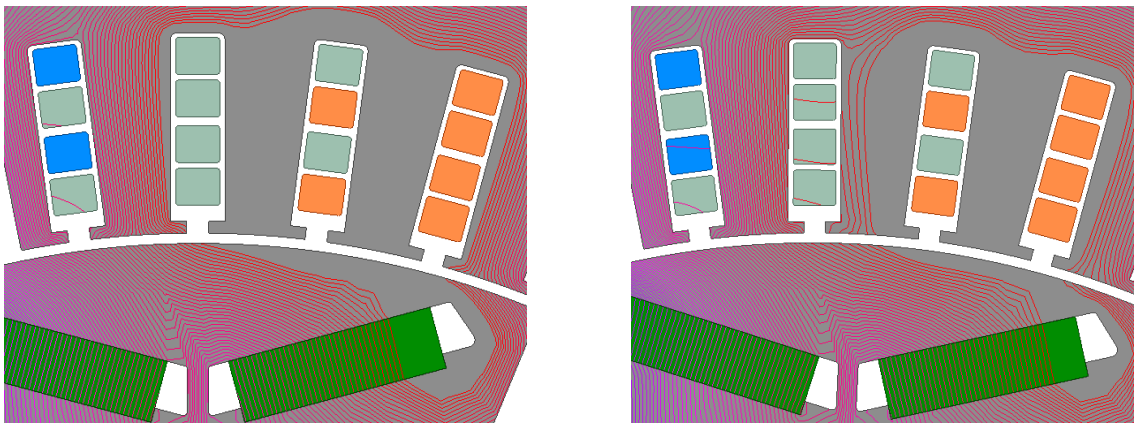

Figure 4.28: Flux lines for full machine at two different current angles, 0 degrees to the left and 10 degrees to the right.

The magnet flux continues to straighten up as the current angle is increasing leading to the case in Figure 4.29 where the MTPA angle, 35 degrees, is used. Now the gap in flux is gone since the peak current slots do not manage to push the flux around them. Also, the leakage flux creating the change in current distribution in the left corner that was seen earlier is visible in conductor B6, bottom green conductor in full B phase. This is dependent on the rotational direction of the machine and would thus be shifted to the right if the rotor was rotating in the opposite direction.

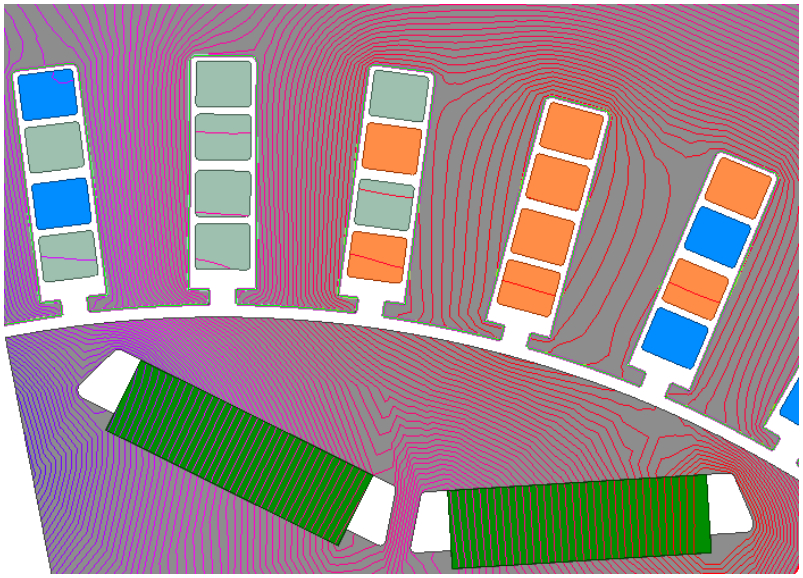

Figure 4.29: Flux distribution in full machine at MTPA angle

This change of current angle is affecting the losses in the conductors since the change

of flux now is lower. In Figure 4.30 the losses in conductor B6 is plotted over one electrical period with the UCD loss as reference. The two peaks are now occurring when the edge of the magnets are passing by the conductor and the magnitude is decided of how much proximity loss that is "available" at that position.

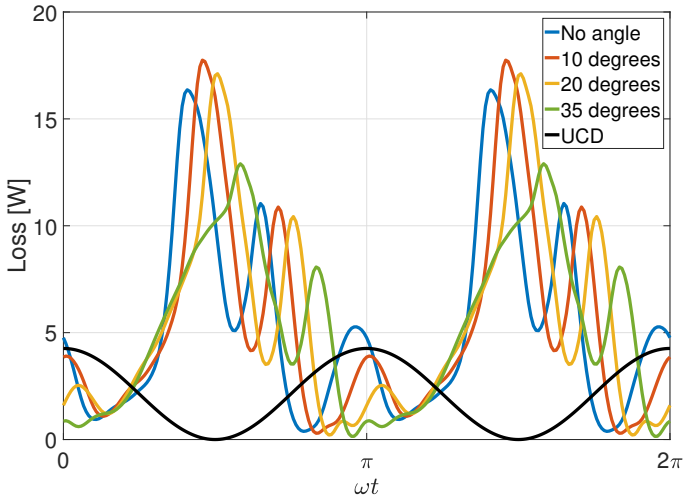

Figure 4.30: Impact of current angle on the AC loss in conductor B6 over one electrical period

Another way to present this is to look at the losses from the rotors point of view. Losses in conductor B6 over one forth of a mechanical period is shown in figure 4.31. The losses occur at the same position, when the magnets are passing the conductor, but the peaks is lowered when current angle is increase. This is due to how large the proximity effect caused losses are at that time. So, to conclude, the losses is now dependent on the position of the magnets instead of only the proximity effect of the conductors.

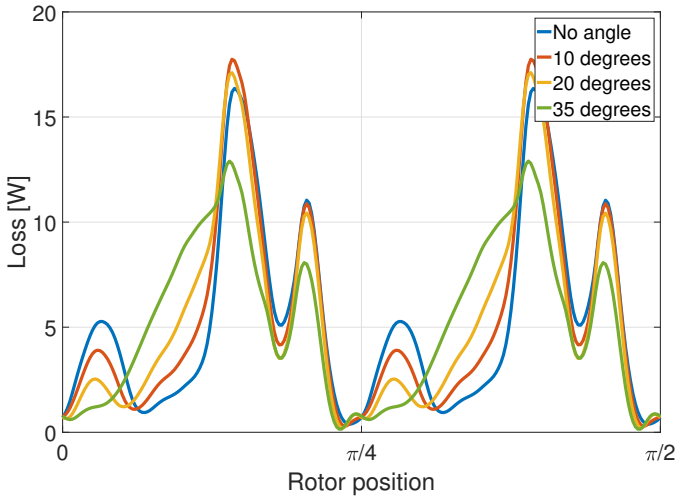

Figure 4.31: Impact of current angle on the AC loss in conductor B6 over 90 mechanical degrees.

The result from the three cases, iron rotor, reluctance rotor and full machine at 10000 rpm is presented in Figure 4.32. This shows that the resistance in the conductors rises for both the case without magnets and the case with magnets. The analytical result for the isolated slot segment is also presented.

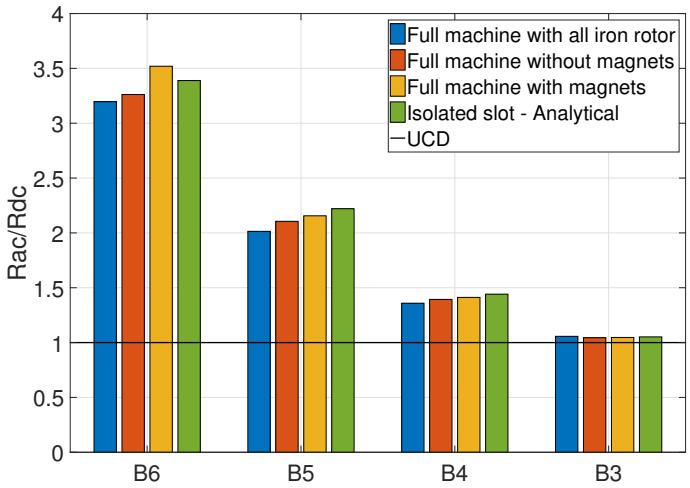

Figure 4.32: The resistance quota for different cases with analytical calculation of resistance.

So, the losses from the isolated slot segment, proximity effect induced losses, is the major contributor to the total loss. Other phenomena are only affecting the losses slightly. The analytical results for the slot segment compared to the FEA results for the full range, 1-2000 Hz, is presented in Figure 4.33.

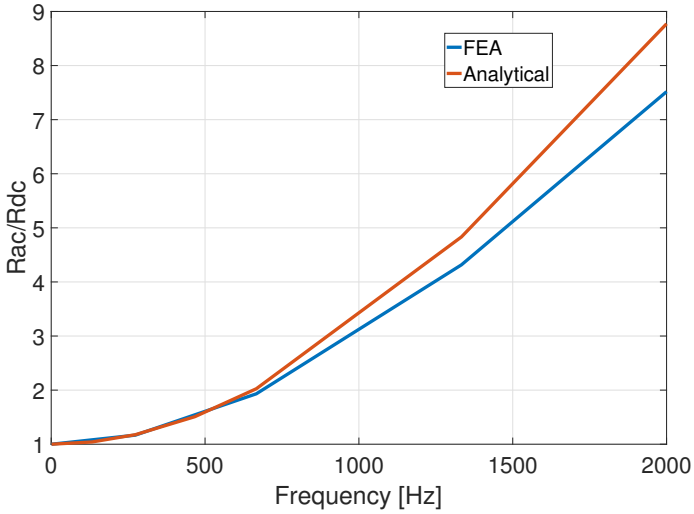

Figure 4.33: The analytical results for isolated slot segment compared to FEA result for full machine

This shows that the analytical expression is over estimating the losses. This is due to that the isolated slot segment are only considering slots with one phase. Since

50% of the machine consist of mixed phases where the losses has shown to be smaller this explains the difference. Note that this is valid for this machine. Other designs might change the losses which would affect the total loss in the machine.

4.3 Impact of design parameter variation

To further deepen the understanding of the increase in resistance of the conductors a test of the influence of two parameters is tested. The parameters tested is the stator slot opening and the number of conductors per slot.

4.3.1 Stator slot opening

The stator slot opening impacts the way the flux chooses since by varying the opening the reluctance is varied. It is affecting a lot of different characteristics of the machine like back EMF, iron losses etc. This section will examine the influence it has on the copper losses and the torque ripple of the machine.

To examine the effect of different slot openings the model is modified to have a slot opening varying from fully closed to fully open. This is done in steps, starting from the fully closed model and then opening the slot by 20% per step until fully open model is reached. The two end position together and the actual machines slot opening, which represents an opening of 40% can be seen in Figure 4.34.

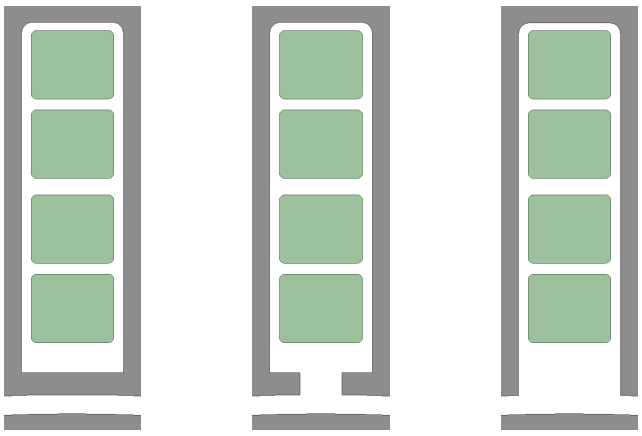

Figure 4.34: Fully closed slot to the left, slot opening matching the Chalmers machine in the middle and fully open slot to the right

The test is performed at *nominal current* and the increase in resistance towards speed for three different slot openings is presented in Figure 4.35.

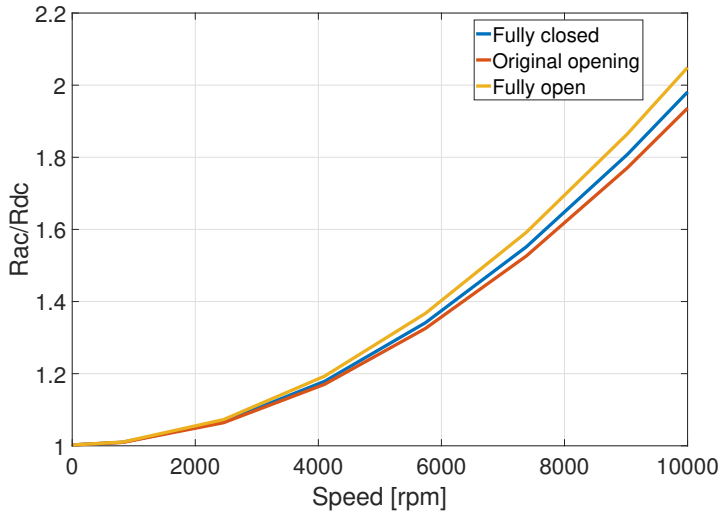

Figure 4.35: Rac/Rdc quota for three different slot openings towards a speed between 15rpm to 10000 rpm.

This shows that the original opening have the lowest resistance for the whole operating range. The biggest difference occur at max speed therefore in Figure 4.36, the resistance quota at 10000 rpm is plotted towards all different openings.

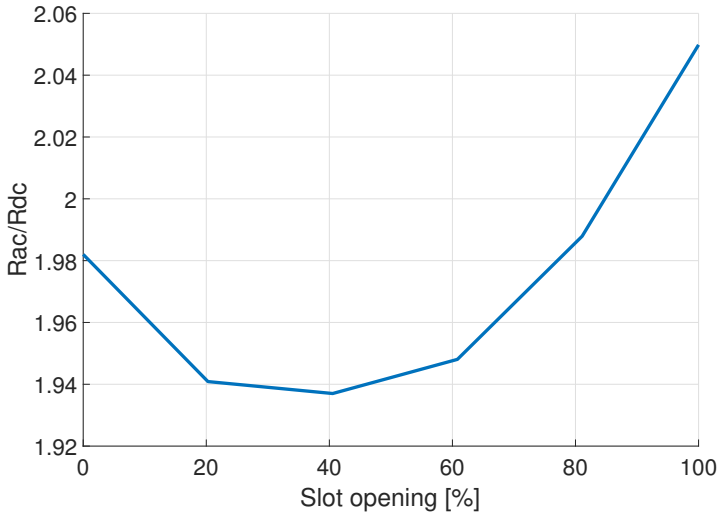

Figure 4.36: Rac/Rdc quota for all slot openings at 10000 rpm

This shows how the resistance is depending on the slot opening. Earlier it has been shown that the resistance increases when more flux is going through the slot. With a larger slot opening the reluctance difference between going through the slot and across the slot opening gets smaller, therefore more flux is going through the slot, causing the resistance to ascend. When making the slot opening smaller and eventually closing it, the reluctance through the shoes is reaching its minimum. Now instead the shoes are saturated making flux to leak through the slot once again.

The slot opening is also impacting the torque the machine develops. The torque towards the different slot openings is presented in Figure 4.37. The torque of the actual machine is used as a reference.

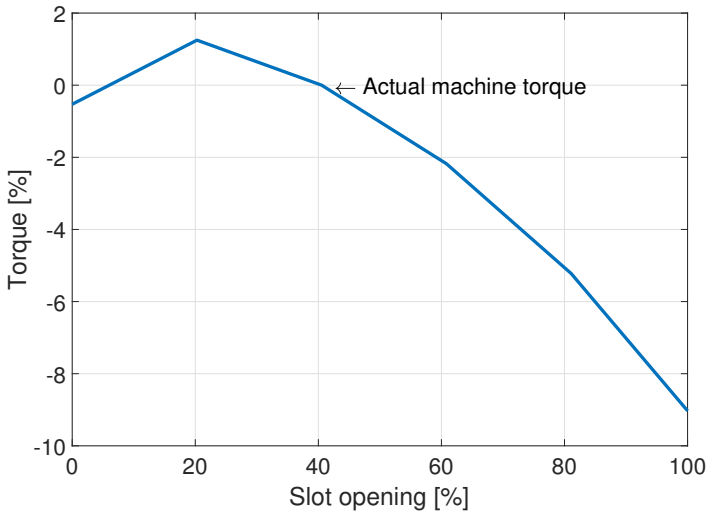

Figure 4.37: Torque ripple vs. slot opening at *nominal current*

This shows that the torque is lowered towards both ends. This is due to that the increases losses is lowering the flux linkage which develops the torque.

The slot opening impacts the slot harmonics that causes torque ripple since a more closed slot make the air gap flux more sinusoidal. In Figure 4.38 the torque ripple is plotted towards the different slot openings. This shows that a smaller slot openings would be preferable to minimize torque ripple.

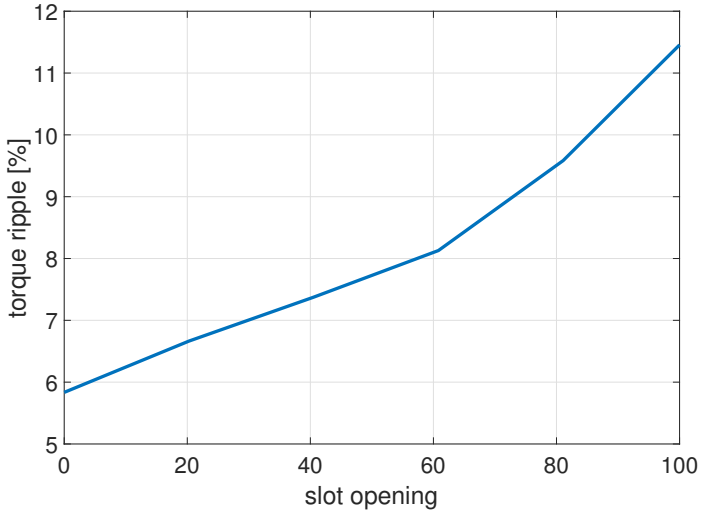

Figure 4.38: Torque ripple vs. slot opening at *nominal current*

4.3.2 Number of conductors

The cross sectional area of the conductors decides the DC resistance of the machine. More, but smaller, conductors decreases the copper fill factor in the slot, since more insulation area is needed, leading to higher DC resistance. As mentioned before the size of the conductors also affects the AC resistance, with more copper that the flux can penetrate, more induced eddy currents, which increases the resistance.

In this test 3 different setups are simulated and evaluated. The 3 setups consist of two, four and eight conductors per slot. To make them comparable regarding the placement in the slot, the conductors have the same width in all cases, thus only the thickness is varied. The thickness is fitted to keep the same distance, 1.1 mm, from the slot opening to the closest conductor in all setups, this leaves the distance of 11.7 mm to be divided in conductors, insulation lacquer and paper. Also, to keep the same torque the total current running in one phase had to be adjusted for the different setups. This gives, using the *nominal current*, $88Arms$, for the four conductor setup, a current of $176Arms$ for the two conductor setup and $44Arms$ for the eight conductor setup. The final setups are depicted below in Figure 4.39 with the actual machine setup is in the middle. The dimensions of the conductors are presented in Table 4.1.

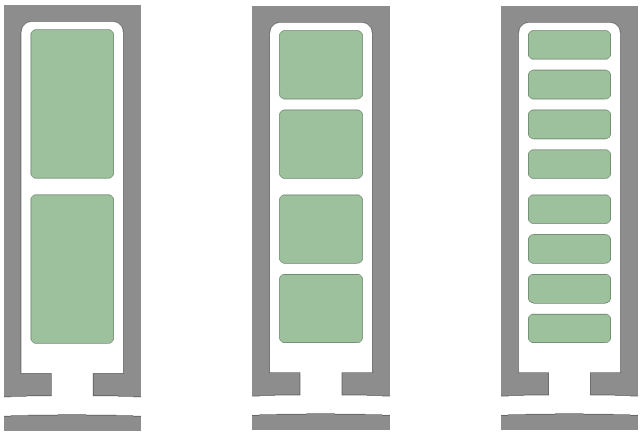

Figure 4.39: The three different setups used for the test. Two, four and eight conductors in one slot

Table 4.1: Dimensions for the conductors in the three different setups

Setup	Thickness [mm]	Width [mm]
Two layer	5.4	3.0
Four layer	2.5	3.0
Eight layer	1.05	3.0

These are all simulated over the full speed range of 15-10000 rpm and the increase in loss is presented in Figure 4.40.

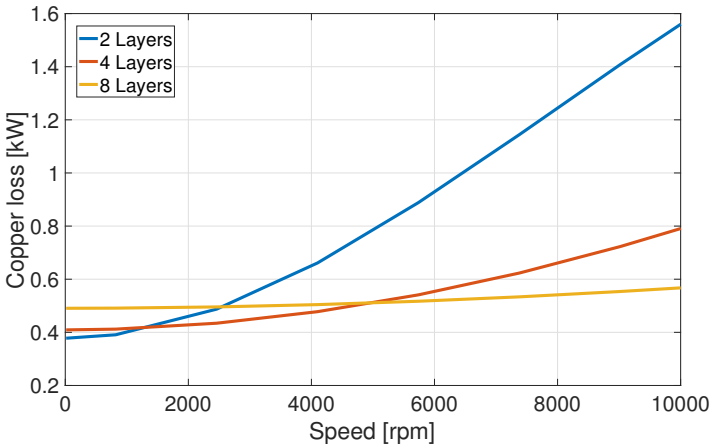

Figure 4.40: Total copper loss in full machine over full operating range

As expected the two layer layout has its losses increasing the most. The eight layer layout is only increasing the losses slightly. Also, the two conductor layout is showing the lowest loss at the lowest speed. The starting loss is only due to the different fill factors, and since less area is used for lacquer and insulation paper, the two layer layout has the highest fill factor. From these losses the resistance of the different setups is calculated and presented in Figure 4.41.

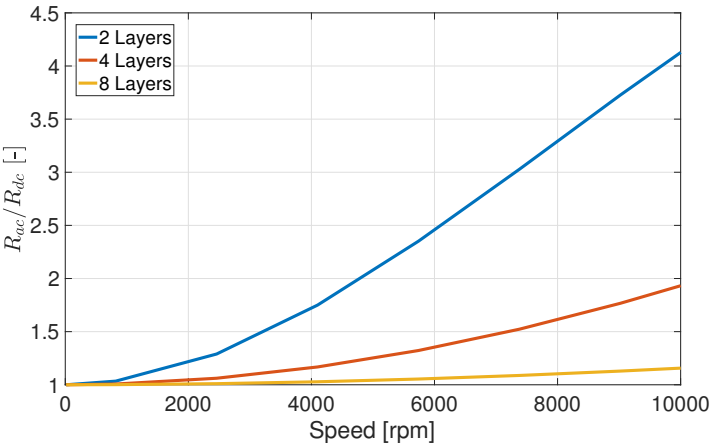

Figure 4.41: Resistance increase over full operating range

4.4 Round winding machine

The round winding machine is also simulated over the range of 1 - 2000 Hz. The resulting copper loss is presented in Figure 4.42. But, remember that the slot area and the amount of copper are not optimised. This would lead to a slightly lower initial loss at zero frequency.

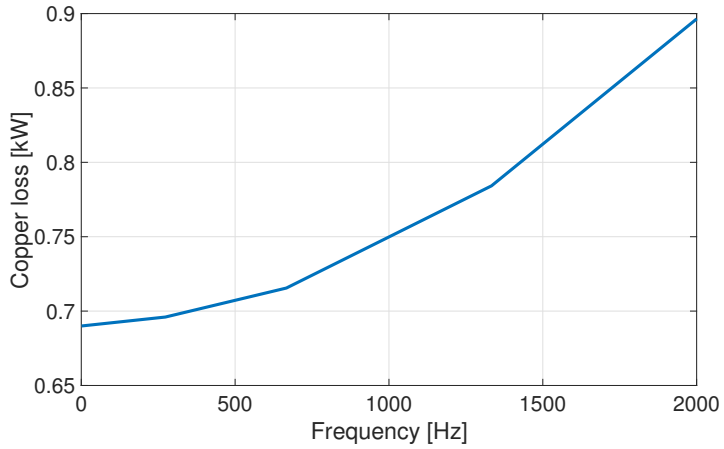

Figure 4.42: Frequency dependant loss for the round winding.

From these losses the frequency dependant resistance is calculated and presented in Figure 4.43. The increase of resistance up to the maximum speed of the machine, at 10000rpm or 666Hz, is 3%.

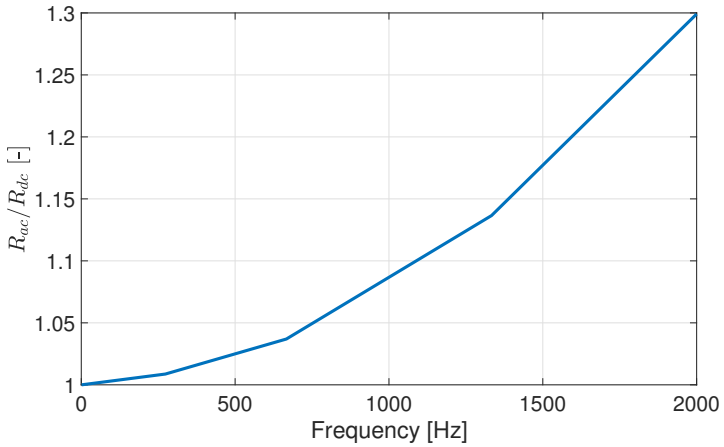

Figure 4.43: Frequency dependant resistance for the round winding.

4.4.1 Comparison of round winding and hairpin winding

To compare the performance of the two different setups the previous results from the simulation of the conductor losses for both hairpin and round winding are compared and presented below in Figure 4.44 for a current magnitude of $88A_{rms}$. It is shown that the total copper loss is increasing faster for the hairpin winding, compared with the round winding type with the increase of frequency. In this comparison it is good to remember that the round winding is not optimised. If this would have been the case the initial loss at zero frequency would decrease for the round winding. But not below the hairpin windings since the hairpin winding still would have a higher amount of copper in the windings.

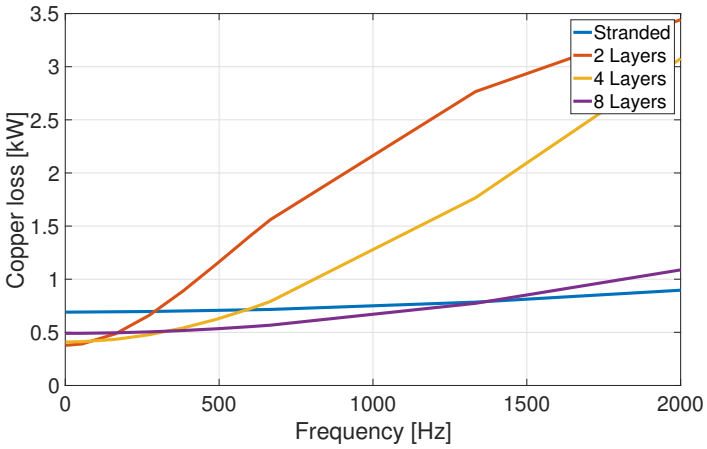

Figure 4.44: Copper loss comparison for the round winding compared to different number of layers for the hairpin machine.

From the losses in the conductors the resistance can be calculated and is shown in Figure 4.45. In this figure the optimisation of the round winding stator would have no, or small, impact on the resistance characteristic for the round winding.

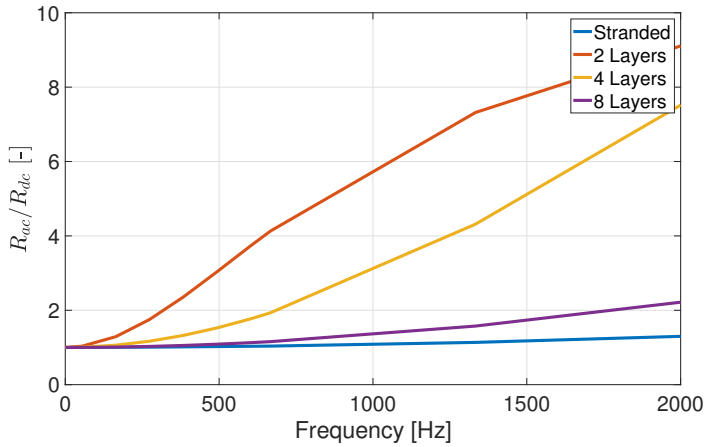

Figure 4.45: Increase in resistance due to speed increase for the round winding compared to different number of layers for the hairpin machine.

As can be seen now in the two layer machine a drop in the increase of resistance occurs. This drop in increase starts at around 700 Hz and is growing with the frequency. This is due to that the skin depth of the two layer machine has dropped to be smaller than the radius of a conductor. This causes skin effect to act on the conductors and together with the other presented effects the resistance increase is now slowing down.

5

Impact of input parameters for simulation

During the simulations some parameters had to be decided. The impact of these parameters is discussed in the following chapter. The parameters of interest is the placement of the conductors in the slots and the impact of not considering field weakening.

5.1 Influence of conductor placement in the hair-pin model

In order to examine the influence of conductor placement in the stator slots four different models is tested, where setup 1 is the layout used for the main results. The placement of conductors in the simulated model is structured, this could be compared with the placement of the conductors in a real machine which will vary due to manufacturing limits. In the manufacturing of the real machine the conductors in the winding could end up not being centered or not being same distance apart from each other since placement of conductors is not completely identical.

The geometrical positions that the conductors has to adhere to is the insulation lacquer layer of the conductor which is set to $0.1mm$ and also the insulation paper thickness of $0.2mm$, this result in a minimum distance between two conductors of $0.4mm$. The insulation paper can be used in different ways, which way that is used in the real machine is unknown at the moment of making the simulation of the conductor placement. Therefore different conductor position is tested. In the test the number of conductors are four as is the case of the real machine and they will be $2.5mm$ x $3mm$, the height of the stator slot is $12.8mm$ and the height of conductors are $10mm$ excluding insulation and paper and this leave $2.8mm$ margin to move the conductors.

No test is done to check how the sideways position of the conductors in the slot affect the results. The width of one slot is $3.7mm$ and the width of a conductor with paper on both sides are $2 \cdot (0.1mm + 0.2mm) + 3mm$ this will leave $0.1mm$ in which the conductor could shift.

5.1.1 Setup 1: Two layer structure with extra paper insulation between conductors 2 and 3 positioned against stator yoke

The real motor consist of two layers of windings consisting of two conductors in each. Since it is not known how the paper insulation is placed an S-shape as assumed around two conductors and then another S-shape is assumed between the remaining two. This results in two paper layers between the two conductors in the middle of the slot. The distance between these two is therefore $0.4mm$ paper and 2x$0.1mm$ insulation. The conductor closest to the yoke is placed $0.3mm$ from the wall and the distance between the other conductors are $0.4mm$. This setup is shown in Figure 5.1.

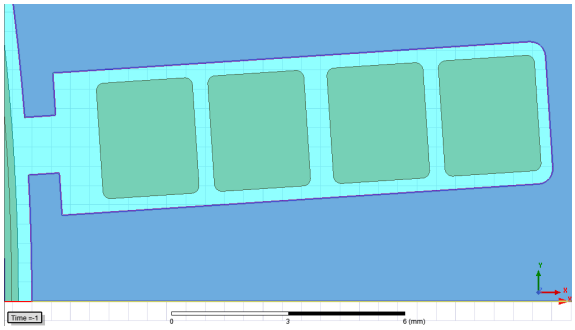

Figure 5.1: The conductors is placed with a minimum distance from each other and placed as close as possible to the yoke.

5.1.2 Setup 2: Two layer structure with extra paper insulation between conductors 2 and 3 positioned against rotor

For this model the conductors are placed in the same way as the previous section 5.1.1, the only difference are that the conductors is placed at a minimum distance from the rotor instead of stator. This setup is shown in Figure 5.2.

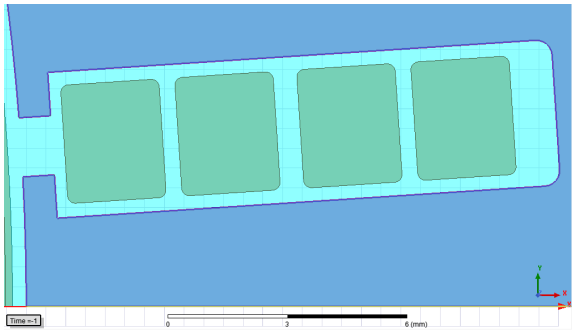

Figure 5.2: The conductors is placed with a minimum distance from each other and placed as close as possible to the rotor.

5.1.3 Setup 3: Even spacing between conductors

In this conductor setup the conductors closest to rotor and yoke is placed one insulation layer plus one paper layer from the walls resulting in $0.3mm$ from walls. This implicate that the distance between conductors is maximised and is $0.73mm$, this setup is shown in Figure 5.3.

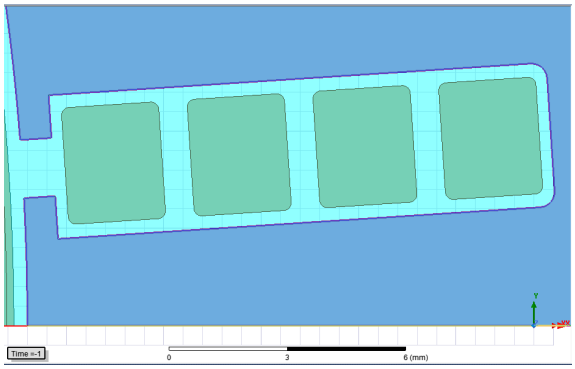

Figure 5.3: The conductors are placed with a maximum distance between each other.

5.1.4 Setup 4: Two layer structure with maximum distance between conductors 2 and 3.

In this setup the conductors placed closest to the rotor and yoke are placed at a minimum distance from the walls, thus maximising the distance between the middle two conductors. This setup is shown in Figure 5.4.

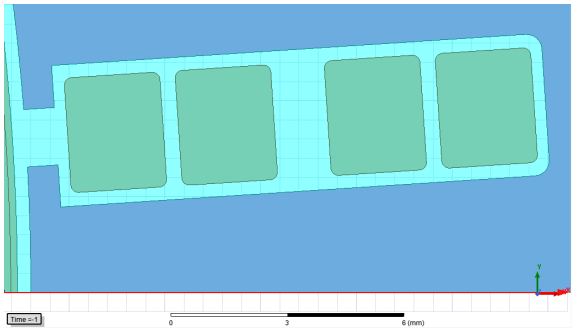

Figure 5.4: Maximum distance between conductors 2 and 3.

5.1.5 Results of conductor placement

The resulting losses for the simulation of different conductor placement is shown in Figure 5.5. The result show that setup 1 gives the lowest losses, about $300W$ lower losses at $30000rpm$. The three other setup has almost equal losses, the highest losses is given when the conductors is placed closest to the rotor. Since the traces are tight to each other also the data for the simulation is provided in Table 5.1.

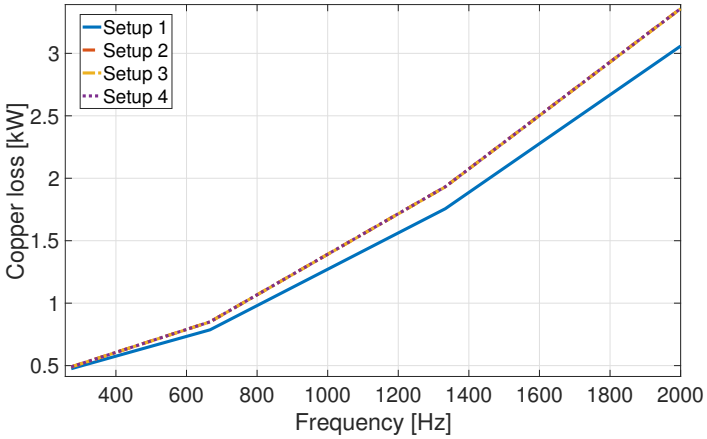

Figure 5.5: Losses for different conductor placement for different frequency.

If setup 2, 3 and 4 are compared, setup 2 has highest loss in the conductors, then setup 4 and after that setup 3. The conductor closest to the rotor is placed at the same position in all setups, the next conductor from the rotor is placed in the same position in setup 2 and 4 which are the two setups with highest losses in the conductors. In setup 3 the second conductor from the rotor is placed further away from the rotor while the third conductor is closer than for setup 4.

From this it may be concluded that the position of the conductor closest to the rotor has the largest impact on the losses. Secondly, the second conductor has the most impact since the losses in Setup 2 and 4 are close to each other. The third and forth conductor does not seem to play such an important role. Which has also been seen in the result chapter.

Table 5.1: Test result for the 4 different conductor placements.

Frequency [Hz]	Setup 1 [kW]	Setup 2 [kW]	Setup 3 [kW]	Setup 4 [kW]
273	0.4754	0.4899	0.4897	0.4899
667	0.7865	0.8507	0.8499	0.8506
1333	1.7563	1.9326	1.9310	1.9325
2000	3.0586	3.3589	3.3567	3.3583

5.2 Impact of field weakening

In the thesis the field weakening has been neglected, this is done by not considering a voltage limit of the machine. If considering a voltage limit field weakening is needed to increase the speed when current and voltage has reached its maximum. To further increase the speed, torque can be decreased by changing the current angle. The changed current angle is lowering the torque, according to 2.9, since i_q decreases, which forces the speed to increase due to $P = T\omega$. When angle cannot increase more the current amplitude is lowered instead this again lowers the torque according to 2.9, which further increases the speed. Together these way of increasing the speed is called field weakening.

So, to conclude the impact that field weakening have is that the current angle increases and the current magnitude decrease while speed is increasing. This section will investigate the impact these two parameters, current angle and amplitude, have on the copper losses.

5.2.1 Current angle impact on copper loss

To examine the impact that the current angle has on the copper loss a study is performed. This study is simulating the machine at maximum speed and at nominal current. The current angle is then swept from 0 to 90 degrees and the resistance change is captured and plotted in figure 5.6.

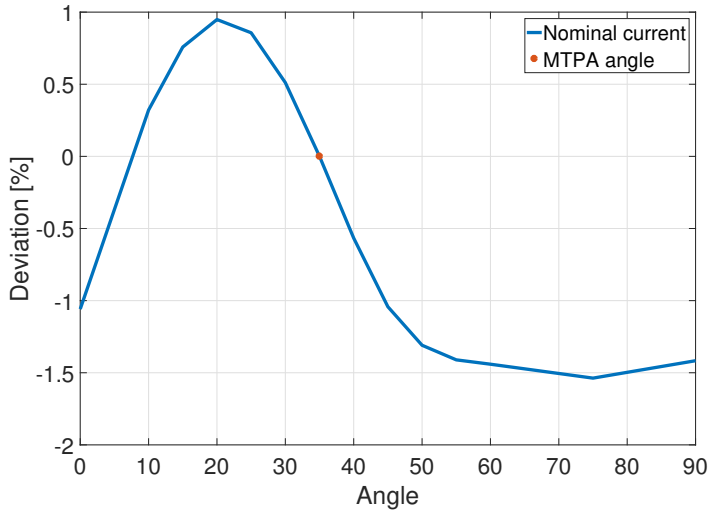

Figure 5.6: Resistance deviation towards current angle. The resistance at MTPA angle is set as reference.

This shows that the resistance is decreasing when increasing the angle from MTPA angle. The resistance is dropping around 1.5% which means that losses decrease with increasing angle.

Also, to find the Maximum Torque Per Ampere (MTPA) angle for any current or setup in the thesis a parametric study was performed. To save simulation time finding the MTPA point the angles in the parametric study was chosen so that the difference between two angles are five degrees. This gives a maximum error of the MTPA angle of two and a half degrees. So when looking at MTPA, the angle to the actual MTPA may differ two and a half degrees. As Figure 5.6 show, an error of two and a half degrees would not impact the losses more than 0.25%. So our simplification of MTPA angle simulation is considered to be okay.

5.2.2 Influence of current magnitude

All tests in this thesis are performed at the nominal current of the machine, this is done to shorten simulation time. If field weakening was to be considered the current

magnitude would need to be changed in the high speed region of the machine. In this section the influence of the magnitude of the current is evaluated. This is done by sweeping currents from 22 A_{rms} up to maximum current of 250 A_{rms}. All currents are simulated at 10000 rpm and at the same angle, 35 degrees. The results can be seen in Figure 5.7.

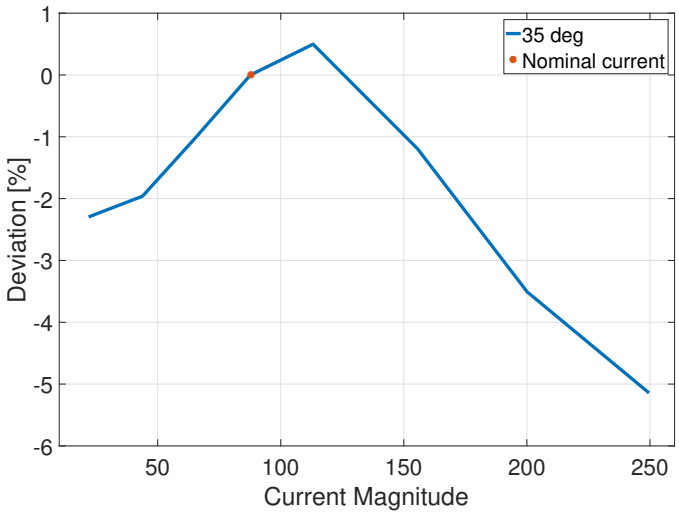

Figure 5.7: Resistance deviation towards current magnitude. The resistance at nominal current is set as reference.

Here it is shown that the resistance is decreasing both for increased and decreased current magnitude. Why this is has not been investigated further but since thermal properties is not considered the resistance at higher current may be changes in real measurements. The resistance would probably be increased due to that the increased losses are increasing the heat developed.

6
Conclusion

This thesis has been focusing on the copper losses and thus the resistance in a hairpin machine and what phenomena that is causing the resistance to change. The study has provided that the resistance in the model of Chalmers hairpin PMSM is increasing with a factor of two when going from low speed, 15rpm to max speed, 10000 rpm.

The eddy effects has been studied and separated in proximity effect, proximity effect between slots, proximity combined with reluctance effect and finally the full machine with the additional effect of the magnets. From this the conclusion that the major contributor to the losses in the hairpin machine is the proximity effect between conductors in the same slot. The other factors are only affecting the magnitude of the losses slightly, their impact is concentrated to when the losses occur.

Another important conclusion that can be drawn is that the losses are focused in the conductors closest to the rotor. The results show that over 40% of the total loss is developed here at maximum speed. This will make cooling a problem since the machine is cooled from the back of the yoke.

Also the hairpins losses are increasing rapidly with speed making it most suitable for low speed applications. While the round random machine is less affected by frequency dependent losses, making it more suitable for high speed applications. Some manufacturers, like Tesla and Jaguar, are using dual motors that are optimised for different speed. This might be a good solution even for the hairpin but further studies are needed.

The comparison between hairpin and round random winding is made using the same sized machine and only changing the windings. This comparison could be made in different ways but this thesis focused on keeping all sizes the same. If optimising the round random machine saturation levels and size would change. A more fair comparison could be included but as the resistance quota would not change notable this approach was considered okay.

7
Future Work

This thesis could be extended in several ways, some suggestions are presented below:

- Use the results regarding losses and also involve thermal behavior of the two machines. Investigate how the temperature dependent conductivity of copper affect the losses.
- Include voltage limits of the design by considering field weakening.
- Excite the machine using a Pulse Width Modulated (PWM) voltage source. This would make it more comparable to a real applications since PWM is the most often used excitation in real applications.
- Perform measurements on the real machine to try to validate the results.
- Extend the analytical model of the resistances to include the impact of mixed slots and magnets.
- Perform simulations over complete drive cycles from real life data. This study has been using mainly the *nominal current* over the full speed range. In a real application the currents, torque and speeds are constantly changing.

Bibliography

[1] IEA. "Global EV Outlook 2018. Towards cross-model electrification". In: *Electric Vehicles Initiative* (2018), p. 143. DOI: EIA-0383(2016).

[2] Christian Du-Bar and Oskar Wallmark. "Eddy Current Losses in a Hairpin Winding for an Automotive Application". In: *Proceedings - 2018 23rd International Conference on Electrical Machines, ICEM 2018* (2018), pp. 710–716. DOI: 10.1109/ICELMACH.2018.8507265.

[3] Wenliang Chen et al. "Strand-level finite element model of stator AC copper losses in the high speed machines". In: *Proceedings - 2012 20th International Conference on Electrical Machines, ICEM 2012* (2012), pp. 477–482. DOI: 10.1109/ICElMach.2012.6349912.

[4] Abdessamed Soualmi et al. "Study of copper losses in the stator windings and PM eddy-current losses for PM synchronous machines taking into account influence of PWM harmonics". In: *ICEMS 2012 - Proceedings: 15th International Conference on Electrical Machines and Systems* c (2012), pp. 1–7.

[5] James Goss et al. "Electrical Vehicles — Practical Solutions for Power". In: 54.3 (2018), pp. 2751–2762.

[6] Dae Sung Jung et al. "Optimum design of the electric vehicle traction motor using the hairpin winding". In: *IEEE Vehicular Technology Conference* 1 (2012), pp. 5–8. ISSN: 15502252. DOI: 10.1109/VETECS.2012.6240320.

[7] Juha Pyrhonen et al. *Design of Rotating Electrical Machines 2 Windings*. Chichester: Wiley, 2010. ISBN: 9780470695166.

[8] Gwendolyn Bailey, Nabeel Mancheri, and Karel Van Acker. "Sustainability of Permanent Rare Earth Magnet Motors in (H)EV Industry". In: *Journal of Sustainable Metallurgy* (2017). ISSN: 2199-3823. DOI: 10.1007/s40831-017-0118-4.

[9] Kim Sang-Hoon. *Electric Motor Control: DC, AC, and BLDC Motors*. 1st. Amsterdam: Elsevier, 2017. ISBN: 9780128123195.

[10] Tae Yong Lee, Yong Jae Kim, and Sang Yong Jung. "Reduction of permanent magnet eddy current loss in interior permanent magnet synchronous motor according to rotor design optimization". In: *9th International Conference on Power Electronics - ECCE Asia: "Green World with Power Electronics", ICPE 2015-ECCE Asia* (2015), pp. 1712–1717. DOI: 10.1109/ICPE.2015.7168008.

[11] Stephen J. Chapman. *Electric Machinery Fundamentals*. 5th. McGraw Hill Higher Education, 2011, p. 768. ISBN: 9780071325813.

[12] Instalaciones Electricas. *Motores eléctricos Las Palmas - Servicios Integrales Todo servicio | Servicios Integrales Todo servicio*. URL: https://www.todoservicio.net/servicios/motores-electricos.

[13] N Mohan, T Undeland, and W Robbins. *Power Electronics: Converters, Applications, and Design*. 3rd. Hoboken, NJ: Wiley, 2007. ISBN: 9780471226932.

[14] D Cheng. *Field and wave electromagnetics*. 2nd. Harlow: Pearson Education Limited, 2014. ISBN: 9781292026565.

[15] ANSYS. "Maxwell Online Help 18.2". 2012. URL: `http://www.ncbi.nlm.nih.gov/pubmed/22451589`.